NASA/TM–20260002810

Results from a Pack-Level Drop Test of Energized Energy Storage System Hardware

Justin D. Littell, Matlock M. Mennu, Nathaniel W. Gardner
Langley Research Center, Hampton, Virginia

May 2026

NASA STI Program Report Series

Since its founding, NASA has been dedicated to the advancement of aeronautics and space science. The NASA scientific and technical information (STI) program plays a key part in helping NASA maintain this important role.

The NASA STI program operates under the auspices of the Agency Chief Information Officer. It collects, organizes, provides for archiving, and disseminates NASA's STI. The NASA STI program provides access to the NTRS Registered and its public interface, the NASA Technical Reports Server, thus providing one of the largest collections of aeronautical and space science STI in the world. Results are published in both non-NASA channels and by NASA in the NASA STI Report Series, which includes the following report types:

- TECHNICAL PUBLICATION. Reports of completed research or a major significant phase of research that present the results of NASA Programs and include extensive data or theoretical analysis. Includes compilations of significant scientific and technical data and information deemed to be of continuing reference value. NASA counterpart of peer-reviewed formal professional papers but has less stringent limitations on manuscript length and extent of graphic presentations.

- TECHNICAL MEMORANDUM. Scientific and technical findings that are preliminary or of specialized interest, e.g., quick release reports, working papers, and bibliographies that contain minimal annotation. Does not contain extensive analysis.

- CONTRACTOR REPORT. Scientific and technical findings by NASA-sponsored contractors and grantees.

- CONFERENCE PUBLICATION. Collected papers from scientific and technical conferences, symposia, seminars, or other meetings sponsored or co-sponsored by NASA.

- SPECIAL PUBLICATION. Scientific, technical, or historical information from NASA programs, projects, and missions, often concerned with subjects having substantial public interest.

- TECHNICAL TRANSLATION. English-language translations of foreign scientific and technical material pertinent to NASA's mission.

Specialized services also include organizing and publishing research results, distributing specialized research announcements and feeds, providing information desk and personal search support, and enabling data exchange services.

For more information about the NASA STI program, see the following:

- Access the NASA STI program home page at http://www.sti.nasa.gov

- Help desk contact information:

https://www.sti.nasa.gov/sti-contact-form/
and select the "General" help request type.

NASA/TM–20260002810

Results from a Pack-Level Drop Test of Energized Energy Storage System Hardware

Justin D. Littell, Matlock M. Mennu, Nathaniel W. Gardner
Langley Research Center, Hampton, Virginia

National Aeronautics and
Space Administration

Langley Research Center
Hampton, Virginia 23681-2199

May 2026

Available from:

NASA STI Program / Mail Stop 050
NASA Langley Research Center
Hampton, VA 23681-2199

Introduction

A new generation of vehicles is being developed to augment the current fleets of aircraft in operation. These vehicles are commonly grouped under electric Vertical Takeoff and Landing (eVTOL) nomenclature and are designed to be fabricated out of composite materials and employ partially or fully electric propulsion systems. Operationally, they are expected to operate with high utilization rates in a variety of crewed and uncrewed mission profiles.

A small number of commercial companies have been developing these vehicles and currently there are only a handful of flying experimental vehicles that exist. However, none have been fully certified for operation in the United States, as these efforts are ongoing. Recently, in order to expedite their development, several companies have been given the authority to begin conducting test flights in the United States as a part of a new Federal Aviation Administration (FAA) eVTOL Integration Pilot Program (eIPP) [1], which is intended "*to accelerate the safe deployment of Advanced Air Mobility (AAM) vehicles in the National Airspace System*." However, even as this program commences, it notes "*The eIPP is focused on informing standards and future policy development and is not a mechanism to bypass certification requirements. Aircraft included in the partnership must already be going through the FAA's formal type certification process."* Restated simply, certification by regulatory bodies must occur before adoptation of these vehicles can be realized. As a part of this certification effort, rules that were originally intended for General Aviation and Rotorcraft aircraft are being reutilized and tailored toward these vehicles. Methods of how these regulations are being utilized for eVTOL vehicles can be found in two examples in the Federal Register [1][3] which describe specifics regarding the certification guidelines under the Special Class or aircraft within 14 § CFR 21.17(b) [4]. It is expected that the certification, at least at the current time of writing, will be achieved through this method.

Regulations pertaining to crashworthiness of Energy Storage Systems (ESS) in eVTOL vehicles appear to be still under development. The ESS system includes items such as Energy Storage Modules (a.k.a. batteries), and all associated hardware to provide the electric power necessary for the vehicle primary propulsion systems. The two regulation examples cited do not explicitly state Means of Compliance for ESS crashworthiness, but instead state (using example ref 3, and reprinted from ref 13) "*risks identified are adequately addressed by the requirements of Subparts E and F, AM1.1529 and Appendix A ICA* (which are already proposed requirements) *for airframe, engines, and propellers, with specific safety objectives*" and that specific Means of Compliance (MoC) will be developed for each aircraft "*with specific safety objectives and means of compliance to address these risks that will be developed and tailored to the specific aspects of the [aircraft].*" This text indicates that regulations specific to ESS still need to be developed.

The European Union Aviation Safety Agency (EASA) has accepted a 50-ft drop test as an acceptable Means of Compliance for ESS systems on VTOL vehicles [5]. The 50-ft standard is based on the fuel tank crash resistance for conventional rotorcraft using both EASA [6] and U.S. regulations [7]. Two Original Equipment Manufacturers (OEMs) have conducted and publicly acknowledged drop tests of their ESS components [8][9]. While the full details of these tests are unknown, and specific results have not been made publicly available, the fact that these tests are being conducted at all illustrates ESS drop tests are under consideration by the eVTOL industry.

Even as the eVTOL industry is conducting testing on ESS components, there are large gaps that exist in the public knowledge base. Having data on ESS components undergoing dynamic tests can help answer questions as to the relevance of the test, the ESS test setup, the ESS configuration and test conduct, the performance of ESS systems under dynamic conditions, the presence (or lack thereof) of hazards that develop and a host of other questions. Having some answers to these questions can help to both further the research being conducted and accelerate certification efforts.

It is from these gaps, along with discussions with various stakeholders, that NASA has decided to undertake research into the crashworthiness of ESS components. As a part of the Revolutionary Vertical Lift Technology (RVLT) project, a team at NASA's Langley Research Center (LaRC) undertook a multi-year research effort. After conducting a background study [10], a three-phase plan was developed. This plan followed a step-by-step process of conducting increasingly complex dynamic drop tests on ESS hardware, starting at the module level and ending with a fully energized pack-level test, replicating, to the best extent possible, an aircraft installation. It is important to note that the goal of the research was not to certify a specific ESS module design or OEM hardware for flight, nor was it to determine packaging designs, features or other components that could offer increased safety for a specific design. Instead, the research was focused on determining the relevance of the test itself to ESS components, highlighting deformation and damage that occurred when components are subjected to various drop and impact variables, associating these mechanisms to distinct factors, and developing a fully functional test as a demonstration of concept by utilization of the data acquired.

This process began in 2023, with Phase 1 drop testing occurring on individual modules without any external hardware present, or attenuation [11][12]. Several tests were completed utilizing various orientations of ESS modules. The results fed into a Phase 2 round of testing, which occurred in 2024 [13]. In this second round of testing, the two worst performing modules were subjected to a “within structure/surrounding structure” configuration (i.e. added attenuation), with acceleration levels purposely chosen to examine whether improvements in performance could be expected. The results of these tests have led the way to a final, pack-level test. This single test was conducted in early 2026 and is described herein.

Test Hardware

The modules that were used for this effort were the same as with previous test efforts to offer comparability between the various phases of test results. Each module was an Electric Power Systems’ (EPS) Electric Propulsion Ion Core (EPiC) ESS, nominally operating at 39 VDC and capable of providing 2.3 kW of power. These modules were designed to withstand TSO-179b [14] and UN38.3 [15] requirements. Six modules were utilized for the test, along with a Battery Management Unit (BMU) and a Mid-point Disconnect (MPD) and all associated power and communication cabling and connections. All modules contained placards displaying “*Not For Flight*”, and had serial numbers (S/N) that were recorded in order to track the individual module results. The six module S/N that were recorded are as follows: S/N 22244-0021, 22244-0036, 22244-0008, 22244-0014, 22244-0010, 22244-0026. For clarity, these numbers will only be referenced by their last four digits in this report. The BMU S/N was 22188-0029 and the MPD S/N was 22193-0001. These three main components are shown in Figure 1.

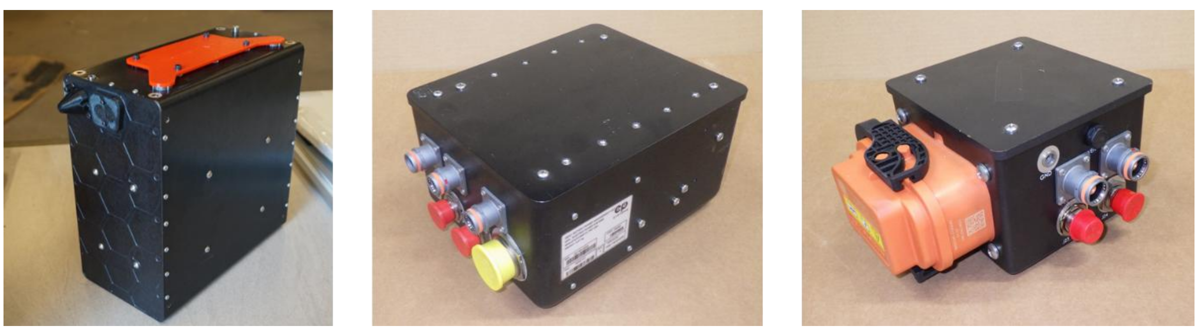

Figure 1. Test Hardware. ESS Module (left), BMU (middle), MPD (right)

Test Background

The development of the test conditions, configuration, and post-test inspections leaned heavily on a mix of the current state of the regulations, the previous phases of testing, and impact data that has been previously collected by NASA in various full-scale crash test programs and vehicles.

The velocity, orientation, and impact surface were chosen to reflect what is stated in the current regulation for Fuel System Crash Resistance [7], which is mentioned in the

Introduction portion of this report. This regulation states the "*most critical tank*" must be drop tested from a drop height of at least 50 feet onto a nondeforming impact surface within a horizontal margin of 10 degrees. These three factors involving the height, impact surface, and horizontal margin have been utilized directly from the regulation and were the basis of the test.

The requirement also states, "The tank must be enclosed in a surrounding structure representative of the installation unless it can be established that the surrounding structure is free of projections or other design features likely to contribute to rupture of the tank." This portion of the text describing the surrounding structure generated a large amount of discussion in the team formulating the test setup; both in how the hardware would be configured and also in what type of impact decelerations would be utilized.

First, a discussion on the decelerations is presented. Deliberations amongst the team members focused on whether having the test articles impact a rigid surface directly would be an unrealistic scenario not found in actual flight operations. Additionally, the data collected from Phase 1 of this series showed accelerations measured during direct impacts on a rigid surface fell out of family with crash pulses developed in full-scale vehicle testing. Furthermore, it was determined that a loading level to represent a more realistic crash condition with the ESS hardware mounted into its surrounding structure should take into account items such as the mounting location in the aircraft (belly, wing, tail, etc.) and the attenuation of loading which resulted from the deformation of the aircraft structure due to the impact. To account for the effect of surrounding vehicle structure on impact acceleration and energy attenuation around the ESS hardware, a pulse generator was included within the test to control the load level into the test article.

The loading levels that would replicate an installation in *surrounding structure* were examined next. A number of tests were consulted when examining the types of accelerations produced in various types of vehicles undergoing crash testing. Data from tests conducted at NASA LaRC provided the source of realistic impact conditions which were then down selected based upon several factors. Two major factors utilized for impact condition development were the data collected from NASA's two Lift+Cruise (L+C) tests, which were conducted in 2022 [16] and 2025 [17]. For the first L+C test (L+C #1), sensors measured acceleration levels both at the bottom skin/belly of the aircraft and at the floor level where the accelerations would be felt by the onboard occupants. The acceleration levels ranged over 140 g at the belly to approximately 40-60 g at the floor level. In the second L+C test (L+C #2), to address some specific concerns regarding belly-mounted ESS systems, there was a specific ESS experiment added to the test to determine loading levels of a rigid underfloor ESS installation. This data from the underfloor ESS experiment produced accelerations similar to the data that was collected in Phase 1 of this research. This was due to the rigid underfloor installation and no energy attenuation present. In the rest of the vehicle, where the energy attenuating subfloor design was installed, the floor level accelerations were approximately 45 to 68 g at various locations, which was similar to those measured during the L+C #1 test.

In the end, a 100-g, 50-millisecond deceleration pulse shape was chosen as the required deceleration input into the test article. These parameters were chosen such that the magnitude enveloped floor level accelerations by over a factor of 2 and assumed the ESS components were installed somewhere other than below the floor. The input pulse magnitude was also intended to be of similar magnitude to inputs that were used in Phase 2 of the research (100 g vs. 80 g in Phase 2). The similar magnitudes provided additional data that can be compared between Phase 3 to Phase 2 results.

The second portion of the *surrounding structure* consideration focused on the amount and type of aircraft structure that would be present for the test. However, because this installation was intended to be vehicle agnostic, aircraft structure such as stiffeners, beams, cables, wires, and other items that could be specific to a make or model of aircraft would not be included for the test. Thus, the *surrounding structure* requirement was addressed via the loading environment only.

The orientation of the modules was the third topic of deliberation among the NASA team. Noting there were only 6 modules to use, questions arose regarding whether they should all be utilized as a single string, two parallel strings, other multiple strings, and then in what orientations those modules would be within the string(s). While six modules are the size of a small pack, it was determined the modules be separated into two packs of three modules each to maximize the amount of data gathered. Each pack was installed in a distinct condition based on the data from Phase 1 and Phase 2. The first condition positioned three of the modules mounted rightside up (with respect to the vent orientation), in a single line, with direct communication and electrical connections. This configuration placed the modules in the orientation with the least amount of damage seen in previous phases of testing, would assess the direct connection links between the modules themselves, and would produce the worst configuration for containment of propagation if thermal runaway (TR) were to occur. The second configuration positioned the modules in a sideways orientation, with cable connections between each of the modules. This configuration oriented the modules in the orientation producing the highest rubric score according to previous phases of testing, and would assess cabling connections during the impact, since by placing the modules sideways, a portion of the cabling would be oriented into the underside of the modules such that cable pull-out would be a concern.

The scoring rubric that was developed and used for previous phases of testing was reused, but with slight changes to how post-test forensic results were handled. The individual modules were not ranked against each other to determine the amount, location and significance of damage that occurred. Instead, the rubric was used more as a guide to focus on the similarities of the component damage or deformation as observed in previous phases of testing as the modules were disassembled.

Test Setup

The test was conducted at the National Institute for Aviation Research (NIAR) utilizing NIAR test equipment and personnel. This setup was conducted in similar matter to the previous phases of tests, which suspended the test article by several cables to a guided trolley that would be released from a height of 50 feet onto a rigid impact surface. The test was conducted in a large outdoor concrete pit to contain potential hazards, should they occur. The test article and trolley were lifted by an overhead hoist and released via a release hook. When released, the test article and trolley would fall freely, guided by wires through the trolley, until contact between the test article and impact surface occurred. The test article was attached such that when contact occurred, the cables connecting the test article to the trolley would go slack and the influence of the trolley motion would be removed. The trolley was stopped via a separate arrestment system which did not interfere with the test article response. This setup is shown in Figure 2.

Figure 2. NIAR Test Setup

A large 0.5-in aluminum base plate was used as the method of attachment for all hardware. The first installed condition positioned the bottom of the three Rightside Up modules onto an interface bar which would then mount directly into the base plate. The second condition positioned the three Sideways modules on the other side of the plate, onto spacer brackets since space was needed underneath the modules to allow for the cabling connections to be made. The BMU and MPD were mounted in the opposite corner, directly onto the base plate utilizing mounting holes in their bases. The layout of all the hardware is shown in Figure 3. Note the vent ports are covered with a protective red vent cap, which was removed to allow for the vent pipes to be attached during the test.

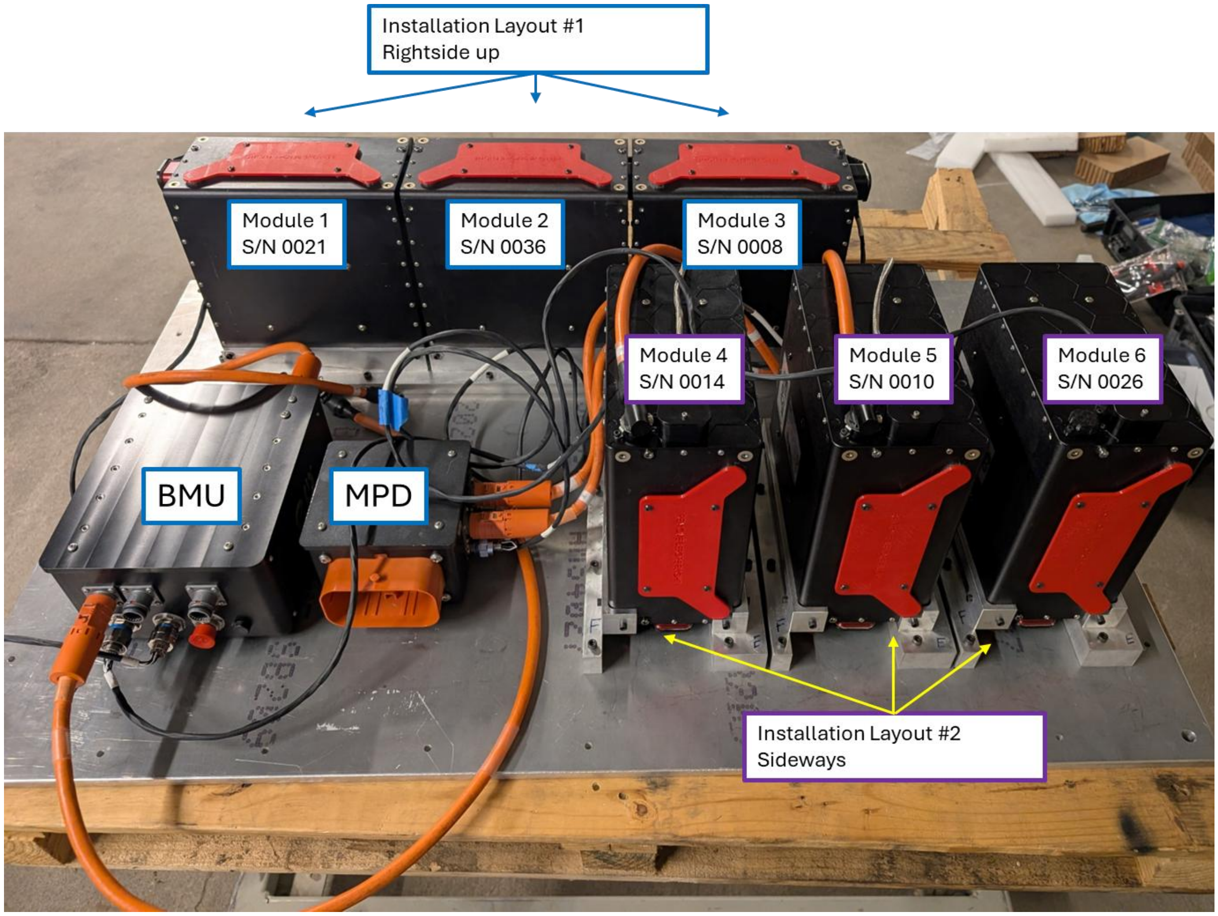

Figure 3. Component layout on base plate

All power and communication cabling was routed wherever possible on the base plate with care being taken not to damage any of the cables. The general routing of the cables started at the BMU and went through the first installation configuration, then to the MPD. From the MPD, the cables went to the second installation configuration and then returned to the BMU.

For the test, ventilation lines were attached to all six modules. The ventilation lines consisted of 2-inch diameter stainless steel tube with custom brackets welded on to interface with each module's vent port. The three Rightside Up modules were grouped and ventilated via a single, continuous ventilation line connected to each vent port, with a 90 degree turn at one end to vent in the same direction as the sideways modules. The Sideways modules each contained their own ventilation line. As with orientations, these two ventilation configurations contained different ventilation types (grouped vs individual), which were chosen intentionally to provide two sets of data to be collected. All lines were ventilated in the same direction to allow for ease of test setup. This single direction is also a feature of an installed condition. To illustrate this setup, a schematic of the ventilation system, which is designated by the purple arrows showing the vent configuration and direction, is shown next in Figure 4.

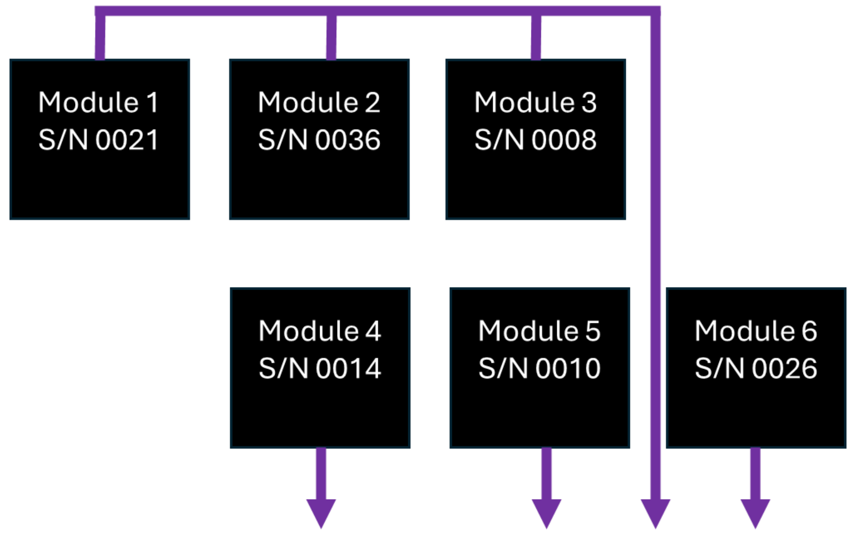

Figure 4. Directional diagram for the test setup ventilation system

Four accelerometers were utilized on the test. A triaxial accelerometer was placed at the center of gravity (CG) on the base plate. Uniaxial accelerometers were placed on the upward facing surface of module S/N 0036, which was in the middle of the Rightside Up modules, and module S/N 0010, which was in the middle of the Sideways modules. An additional uniaxial accelerometer was mounted to the upward facing surface of the BMU. Thermocouples (TCs) were fastened to all of the individual modules in the middle of the broadest side. All instrumentation was connected to an offboard data acquisition system (DAS). The acceleration data were collected at a rate of 100 kHz, while the thermocouple data were collected at 5 Hz. The DAS was controlled via a start trigger that would initiate when the drop trolley crossed a height threshold immediately before impact.

Unlike previous phases of testing, there was real time data available from the BMU that gave indication of the state of charge, faults, and general status of each of the 60 individual cells in the entire module chain prior to, during, and after the impact. The BMU was connected to an offboard computer via an added umbilical to the main DAS data cable. While the system recorded a host of system parameters, it had a low data collection rate of approximately 0.5 Hz. Even with this low data rate, it was able to capture many parameters that would not have been otherwise obtained. The BMU was also used as a secondary method for monitoring the status of the modules for the hour of active monitoring that occurred post-test.

Several high-speed cameras were positioned around the impact location, as shown in Figure 5. The cameras were synchronized with respect to each other and shared a common, middle-trigger recording function, such that half of the data is recorded prior to the trigger and half of the data is recorded post-trigger. The trigger initiated when the drop trolley crossed a height threshold immediately before impact.

Two high-speed cameras were positioned at isometric angles around the impact site. One was positioned on the Northwest side of the impact site, near the corner and angled to view the North and West sides of the ESS hardware (BMU, MPD and three Sideways facing modules). The second high-speed camera was positioned on the Southeast side of the impact site, near the corner and angled to view the South and East sides of the ESS hardware (single Sideways module and three Rightside Up modules). A total of four high-speed cameras were utilized for high-speed photogrammetry, including marker tracking and three-dimensional Digital Image Correlation (3D-DIC). One pair of high-speed cameras was positioned in a stereo configuration perpendicular to the East face of the ESS and viewing the surface of the Rightside Up modules. The other pair of high-speed cameras was positioned in a stereo configuration perpendicular to the South face of the ESS and viewing the surface of the Sideways modules. Finally, a single high-speed camera was positioned on the North side of the impact site, providing complete coverage of the ESS hardware from all four cardinal directions.

The camera resolution was set to between 0.5 and 1 megapixels (MP) depending upon the camera system used and the desired application. The higher resolution cameras were used for photogrammetry, while the lower resolution cameras were used for general ESS viewing. The cameras were set-up to acquire images at 10 kHz with a continuous write-overwrite loop to the cameras buffer until the trigger event. Total recording duration varied between the camera systems based on the available volatile memory of each camera used.

Two infrared (IR) cameras were positioned around the impact site to measure temperatures on the ESS components during the test. One was positioned on the Northwest side corner, angled and capable of providing thermal results for the North and West sides of the test articles, which were dominated by the Sideways modules. The second camera was positioned on the Southeast side of the impact site, near the corner and angled to capture data on the East and South sides, which were dominated by the Rightside Up modules. A schematic of the camera setup is shown in Figure 5.

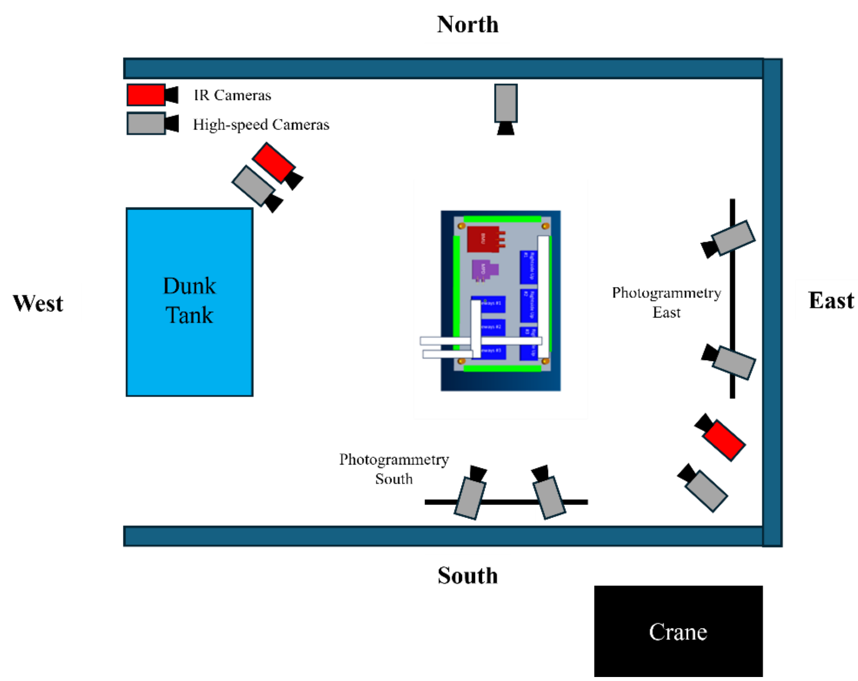

Figure 5. High-speed and IR Camera Layout

Specimen preparations were completed to allow for the 3D-DIC data to be obtained. Prior to testing, the modules were wiped clean to minimize any surface contamination. A thin base coat of white paint was applied, providing a uniform high-contrast background. Note, the surface of the modules, as well as all terminals, connection points, venting tubes, BMU and MPD, were masked off to prevent overspray contamination. A random, black stochastic speckle pattern was applied to the surface using a custom-made vinyl stencil pattern with a speckle size ranging from approximately 1/8 to ¼ in. The speckle patterns on the Rightside Up and Sideways battery modules are shown in Figure 6.

Figure 6. Speckle pattern on battery modules for 3D-DIC. Rightside Up (Left) and Sideways (Right)

Once the speckle pattern was applied, and sufficient time had passed to allow for the paint to dry, yellow and black bowtie markers were positioned at specific locations for marker tracking. Bowties were positioned on the ESS hardware and the guided drop trolley, as shown in Figure 7. After the bowties were positioned and affixed, the distances between each bowtie were carefully measured and recorded.

Figure 7. Bowtie marker positions on guided drop trolley and ESS hardware

The base plate was ballasted to achieve a CG at its geometrical center. Ballast in the form of steel blocks were placed in the corner closest to the BMU. Posts with swivel hoist rings were added to the corners of the plate to interface with the NIAR lifting system. A protective cage was mounted to the posts in order to shield the modules from damage due to the falling trolley or any of its components or from the test article landing in a position other than upright, which occurred in previous tests. Angle brackets were applied to three of the four sides of the baseplate which added stiffness to the plate and provided a location to place the bowtie markers to be used by the high-speed camera systems. Paper honeycomb stacks were placed underneath the plate to act as the acceleration pulse generators. The test article was positioned such that the Rightside Up modules (Modules S/N 0021, S/N 0036 and S/N 0008) faced East, with the outlets of the vent tubes facing West. This orientation positioned the positive x-axis of the test article facing East, and the positive y-axis of the test article facing North. Noting all the additions, the final weight of the test article was 361.4 lb., with the CG centered on the plate. The East side of the test article is shown in Figure 8, the West side of the test article is shown in Figure 9 and the top of the test article is shown in Figure 10.

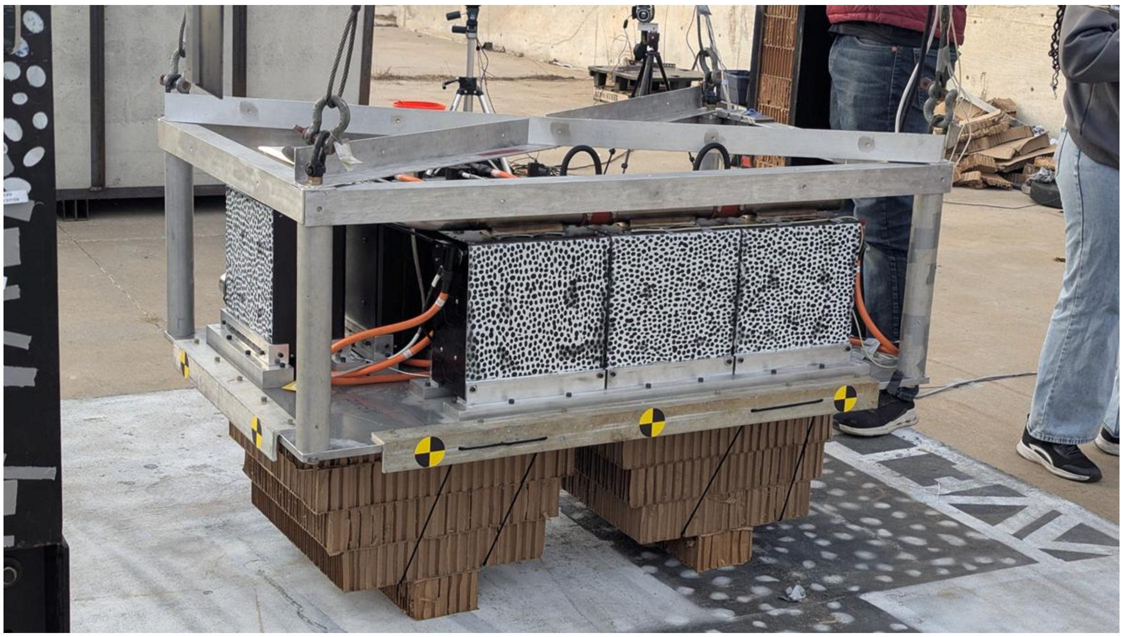

Figure 8. Test article - East face

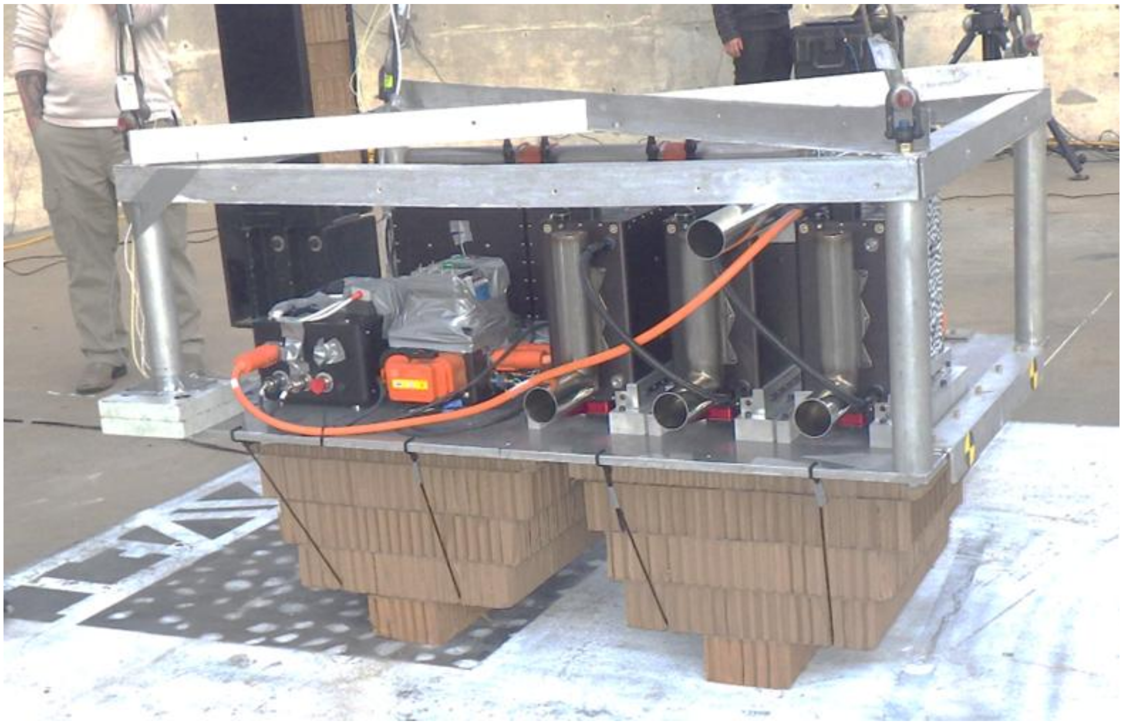

Figure 9. Test article - West face

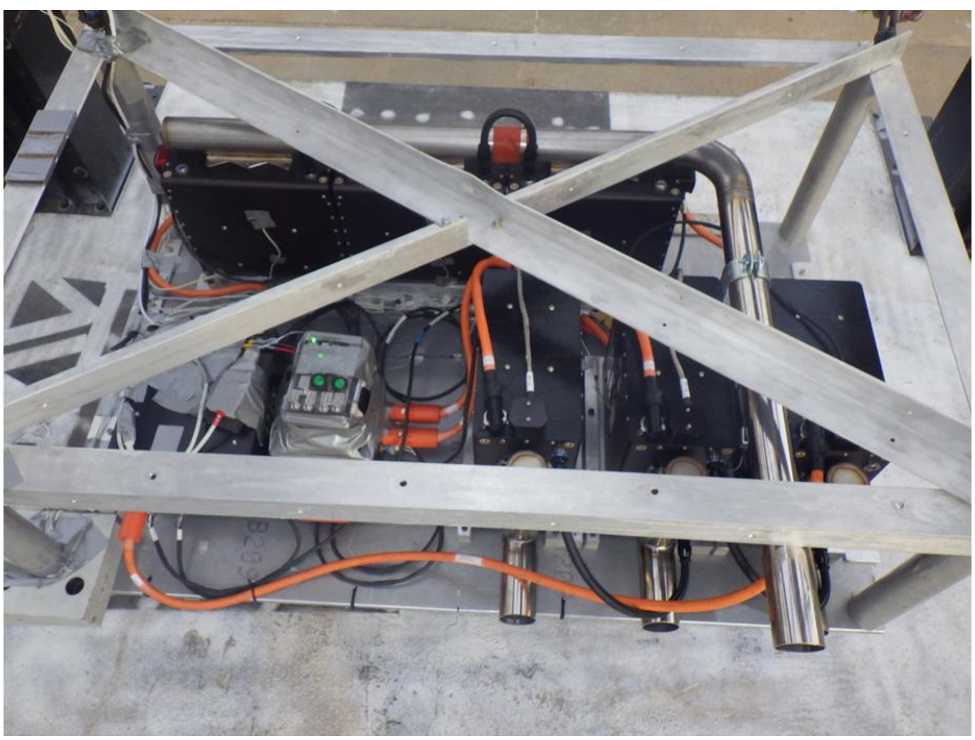

Figure 10. Test article - Top

Finally, for the test, there was no “load” on the system, meaning there was no external component drawing power from the modules themselves. Additionally, the BMU contactors were placed in a closed position during the test. The modules were charged to be as close to 100 % State of Charge (SoC) as possible, and were tested at 96% SoC, with a total voltage of 265.4 volts DC (VDC). Pretest checkouts were completed at 4:38 PM local time with this configuration and no faults in the BMU data occurred. There were two TCs that had no signal on the DAS – TC 2 located on module 2 S/N 0036 and TC 5 located on module 5 S/N 0010. The lack of signal was indicative of a connection break somewhere between the sensor and DAS, however the decision was made to continue the checkouts and conduct the test using only the other four TCs that were providing readings, and to forgo further troubleshooting on these two sensors. The four live TCs measured temperatures between 14.2 and 16.6 ° C on the instrumented modules. After final pictures were taken, the test article was lifted to the 50-ft drop height.

Test Results

The drop test occurred on January 13, 2026, at 5:19 PM local time, which was approximately 41 minutes after pre-test checkouts. The temperature was 56° F with calm winds. The test article impacted with a vertical velocity of 55.6 feet/second with a 1.5-degree North-side low angle, which represented negative rotation about the x-axis, and 2.7-degree East-side low angle, which represented positive rotation about the y-axis. An image sequence, as taken by a high-speed camera located South of the impact is first shown in Figure 11.

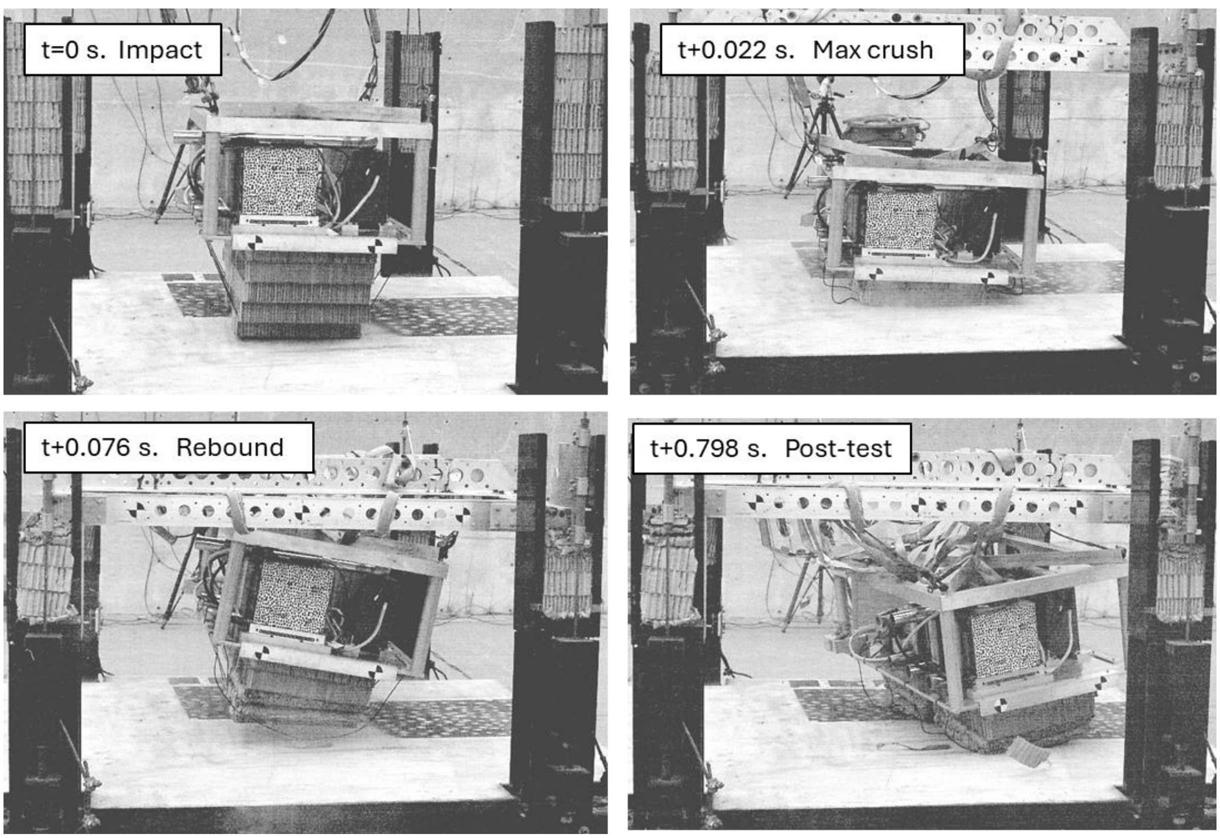

Figure 11. Image sequence - South view

The image sequence shows the test article impacted at an East-side-low angle (positive y-axis rotation) of 2.7 degrees. The honeycomb began to crush, during which the test article appeared to stay at an East-side-low, but relatively constant angle. The crushing lasted approximately 0.022 s, after which the test article began to rebound. At 0.076 s after impact, the test article fully rebounded off the impact surface, still under an East-side-low angle. The test article recontacted the impact surface approximately 0.59 s after impact, which is not shown in Figure 11, and came to rest after rocking to an East-side-high angle approximately 0.798 s after impact. There were no notable events that occurred with the visible modules in the south camera view, other than that they followed the gross motion of the entirety of the test article. The East view was next examined, and an image sequence of this view is presented in Figure 12.

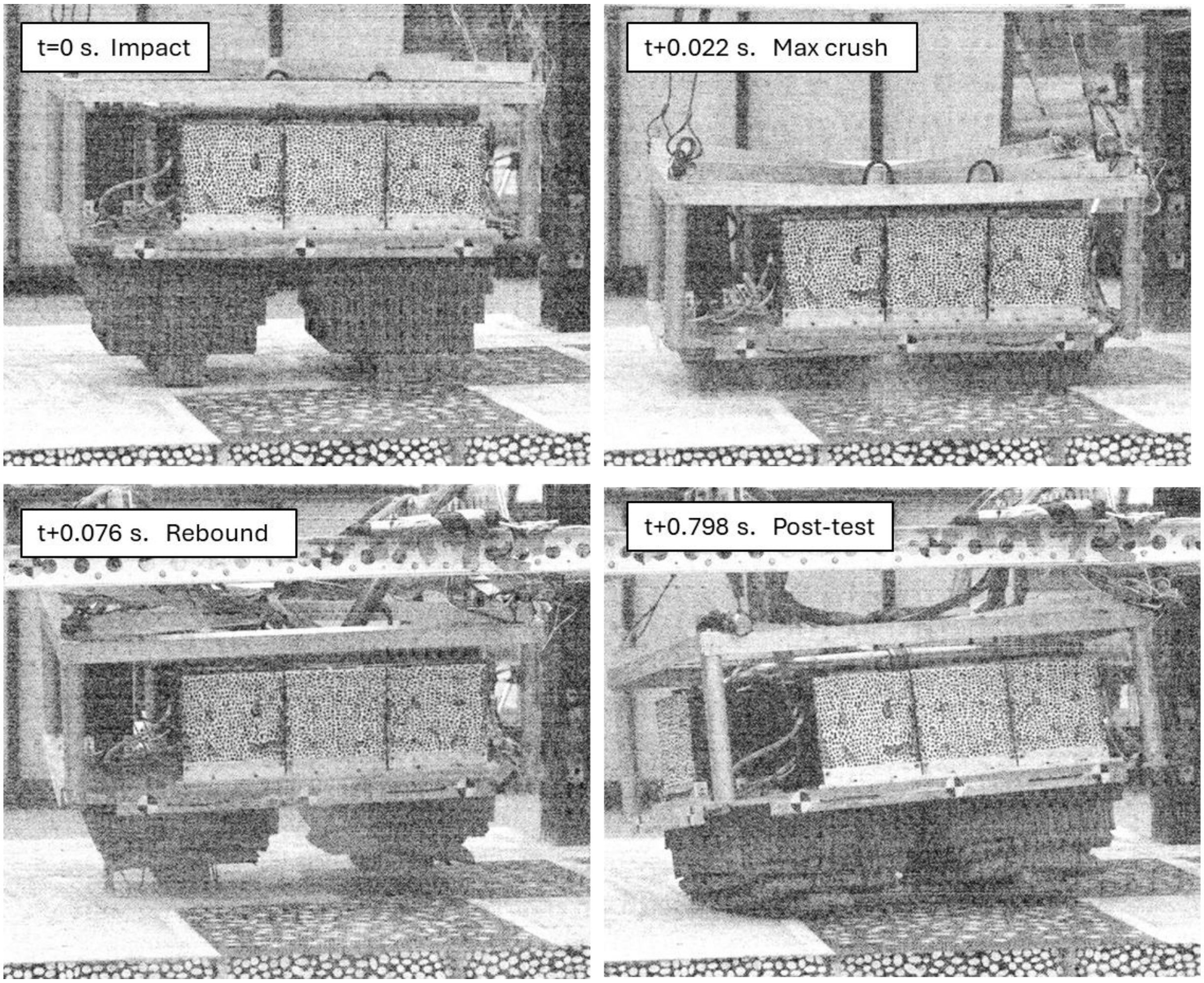

Figure 12. Image sequence - East view

The East side image sequence shows the test article impacted at a slight North-side-low (negative x-axis rotation) angle of 1.5 degrees. The honeycomb began to crush and continued to crush uniformly until maximum crush was reached (t + 0.022 s). Afterward, during the rebound, the test article began to exhibit a South-side-low angle which remained through the entirety of the test and is evident in the post-test orientation of the test article (t + 0.798 s). There was no notable event that occurred in the visible modules; however, it appeared the protective cage had buckled inward during the initial crushing of the honeycomb. Through inspection of the high-speed video, the protective cage appeared to buckle due to the base plate flexing during the crush event.

After the impact and the active post-test monitoring, the test article was approached and visual inspections occurred. An image of the East side of the test article is shown in Figure 13. The West and South faces are shown in Figure 14, and the North face is shown in Figure 15.

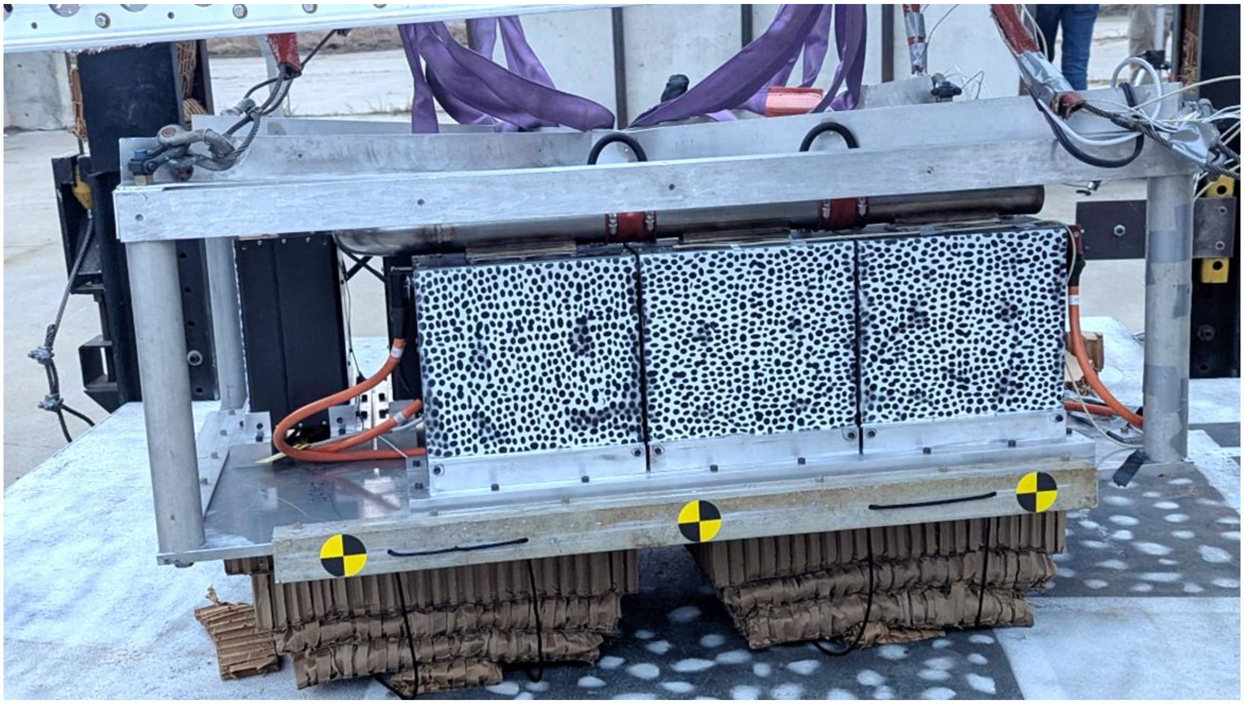
Figure 13. Test article - East face, post test

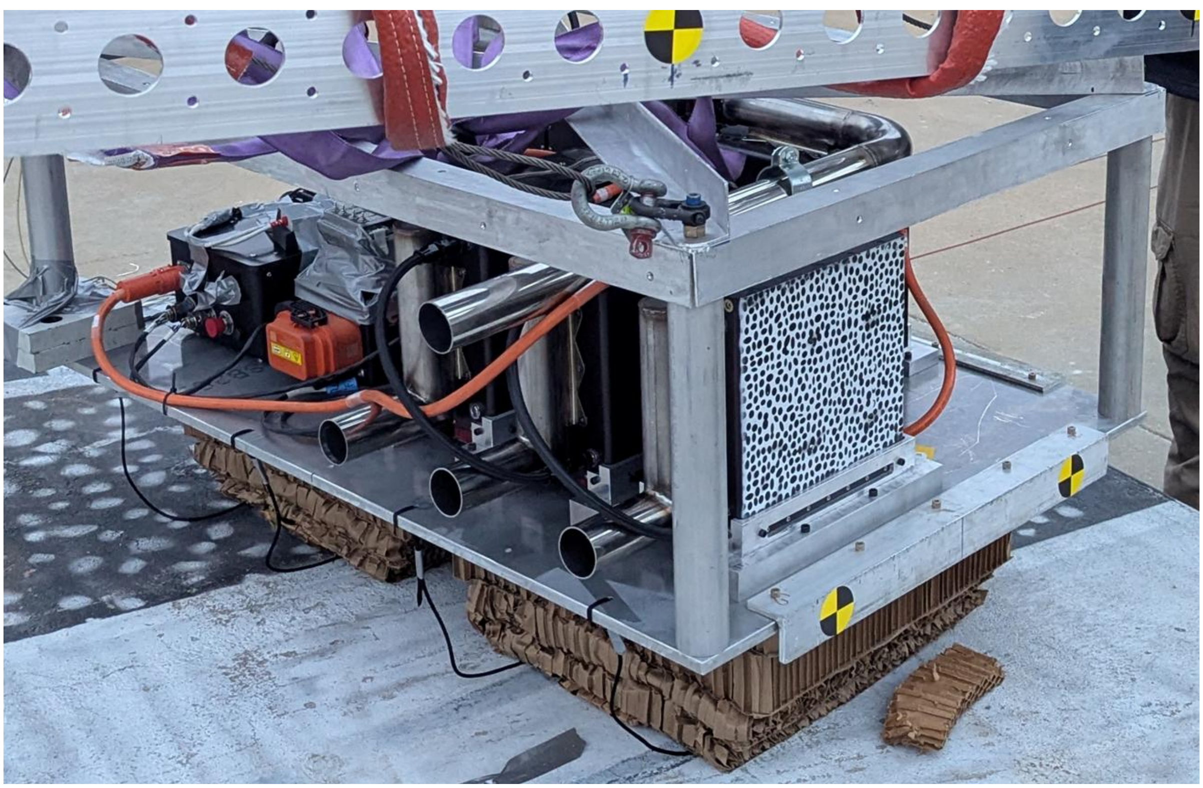
Figure 14. Test article - West and South faces, post test

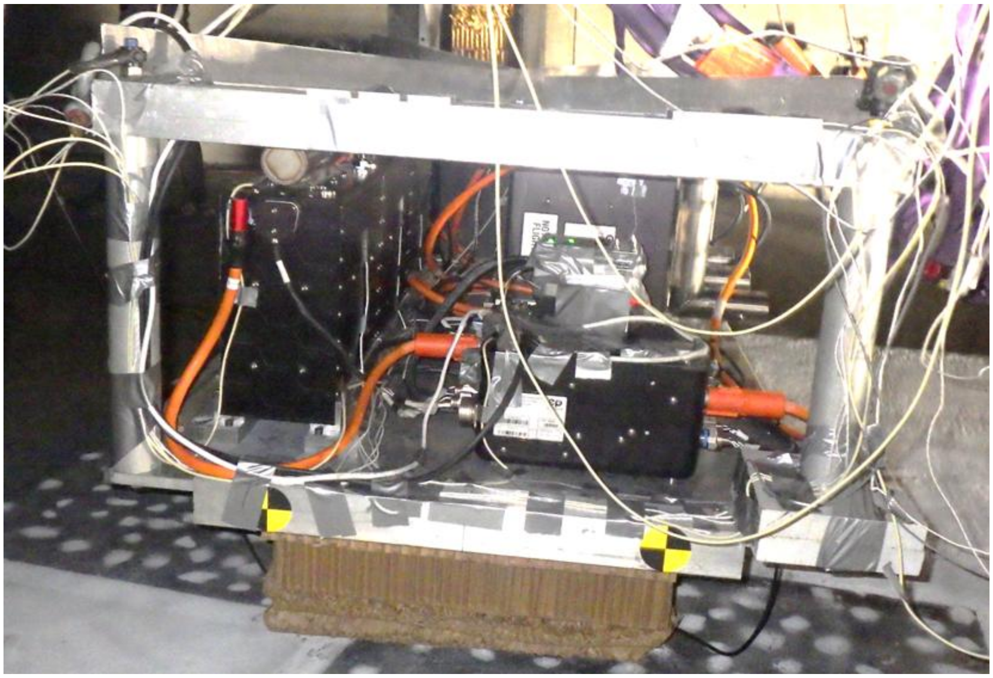

Figure 15. Test article - North face, post test

The visual inspections post-test revealed no major damage in the test article, other than some bending in the top of the protective cage. As noted previously, this was likely from the base plate flexing during the honeycomb crush. However, it appeared this bending did not affect module response, and the cage was still capable of acting as a protective barrier for the drop hardware associated with the drop trolley. All the modules, BMU, and MPD, along with cables appeared to be undamaged during the visual inspections and none of the mounting hardware, which included both the bolts and the brackets, was loose or missing. The overall first impression was that the test article remained intact from the test. However, post-test processing of the data would validate or invalidate this conclusion. The vertical acceleration data were first examined. The filtered acceleration data are shown for all four locations in Figure 16. Note that all acceleration data presented are filtered using standard filters as defined in SAE J211 [18].

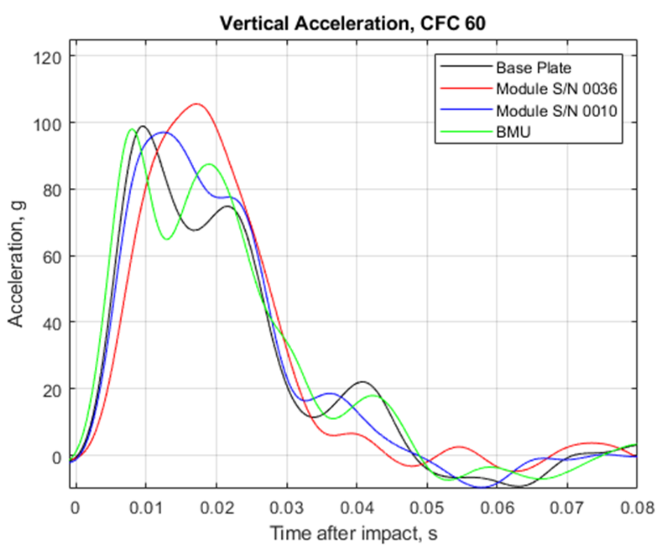

Figure 16. Vertical acceleration

The vertical acceleration data showed the magnitudes reached expected values of approximately 100 g. The BMU and baseplate exhibited similar shapes of response, both having initial peaks followed by a local minimum before rising again to a second peak value before unloading. For the BMU the initial peak value was measured to be 97.9 g and the second peak was 87.5 g prior to unloading. For the base plate, an initial peak value of 98.8 g was observed, which occurred 0.009 s after initial contact. The base plate also experienced a local minimum before reaching a second peak value of 74.8 g prior to unloading of the plate. The two modules measured similar magnitudes, but less of a two-peak response. The response more resembled a half-sine shaped curve with single peak values of 97.0 and 105.5 g, for Module 2 (S/N 0010) and Module 5 (S/N 0036), respectively. In all instances, the duration of the pulse was approximately 0.03 s for most of the response, after which trailed in a shallow path toward the zero-crossing at approximately 0.05 s. Since the test article impacted with slight off-axis angles, the lateral accelerations were also examined. These are shown next in Figure 17.

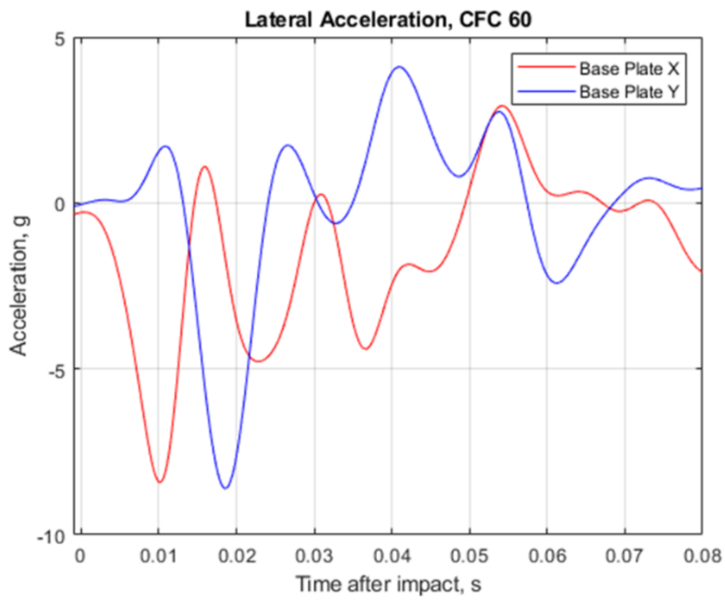

Figure 17. Lateral accelerations

There are single large spikes in acceleration for each of the lateral directions. In the X direction, the absolute magnitude of acceleration was 8.4 g, which occurred 0.010 s after impact. In the Y direction, the absolute magnitude of acceleration was 8.6 g, which occurred 0.018 s after impact. Looking back to the vertical acceleration, the maximum X value occurred at the same approximate time as the initial peak values, and the maximum Y acceleration occurred at the same approximate time as the second peak values. Furthermore, all these values occurred before maximum crush (t + 0.022 s), which was confirmed by examination of the high-speed camera data. The time difference in peak X and Y accelerations confirm a slight angle in the base plate at the time of impact.

Marker tracking was used to track the two-dimensional position and motion of bowtie markers throughout the time-history of the event. Typical marker tracking analysis is shown in Figure 18 and Figure 19, which was used to calculate the impact conditions. Using the East-side camera system, the vertical velocity and North-to South (x-axis) angle were calculated by tracking the bowties that were positioned on the ESS hardware. Using the South-side camera system, the vertical velocity and East-to-West (y-axis) angle were calculated. Note, the vertical velocities, as well as the X- and Y-angles, were also calculated for the guided drop trolley for comparison and to provide confidence in the measurements. Note in the plots below, all angles are presented as a positive value, with their direction being signified in the text.

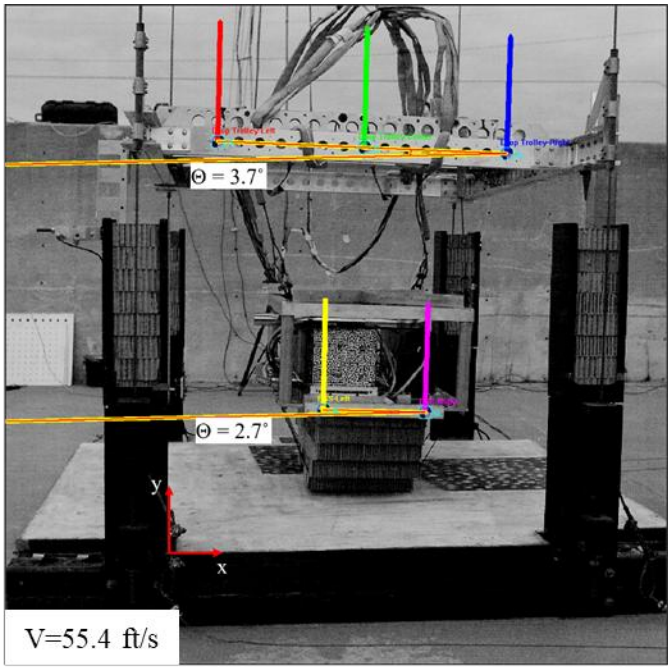

Figure 18. Impact conditions for South-view camera systems (Sideways module)

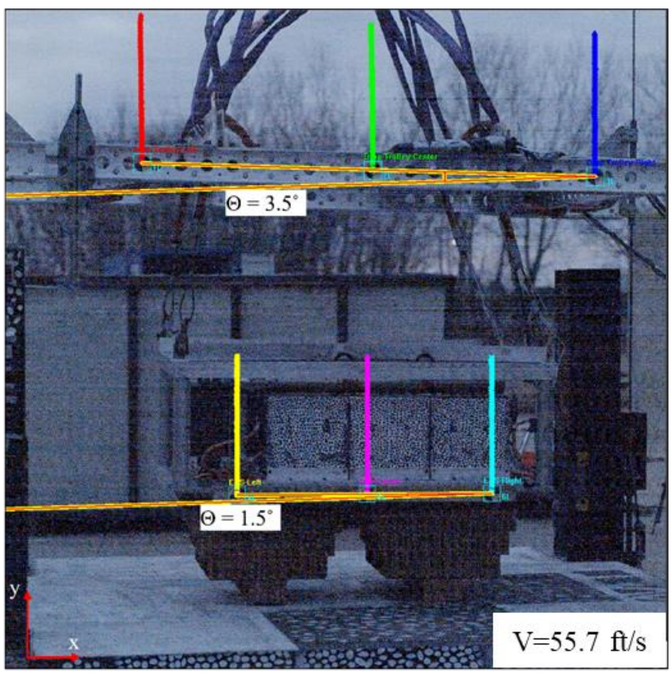

Figure 19. Impact conditions for East-view camera systems (Rightside Up modules)

The 3D-DIC results are shown next in Figure 20 through Figure 25. The in-plane (vertical) and out-of-plane deformation contour plots for the Sideways modules (South-view camera system) are shown in Figure 20, along with the time-history of average displacement, Figure 21 and Figure 22. The purple color represents the minimum value, while the red color represents the maximum value.

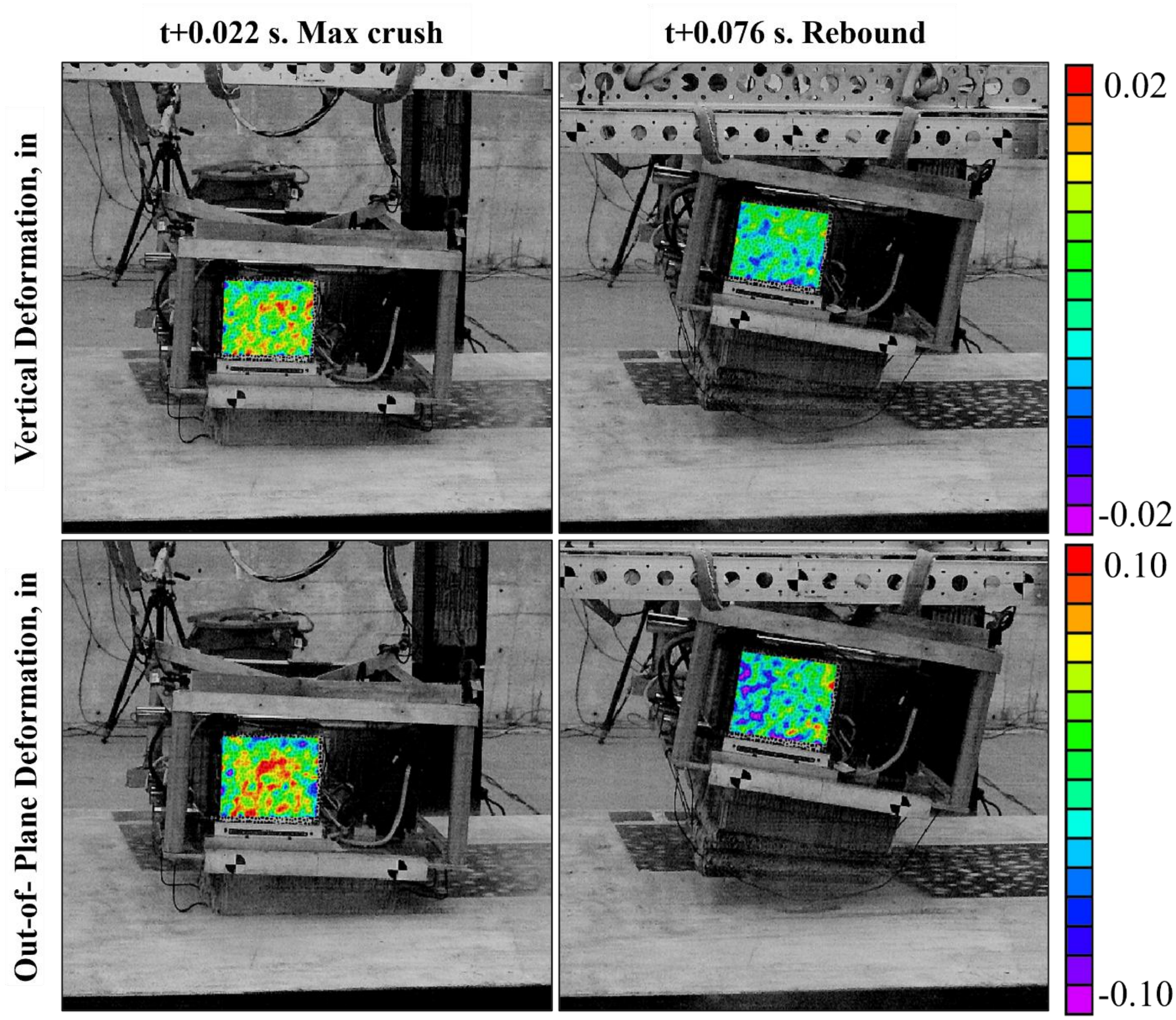

Figure 20. In-plane (vertical) and out-of-plane deformation contour plots for Sideways module (South view)

The Sideways module exhibited a very rigid response and deformation by noting the small values of deformation that occurred. The overall magnitude of vertical deformation and out-of-plane deformation was approximately ± 0.02 inches and ± 0.10 inches, respectively. An examination of the time-history of the average displacement, as measured across the entire surface of the module, provides a more complete understanding of the overall response. The time-history plots are shown next in Figure 21 and Figure 22.

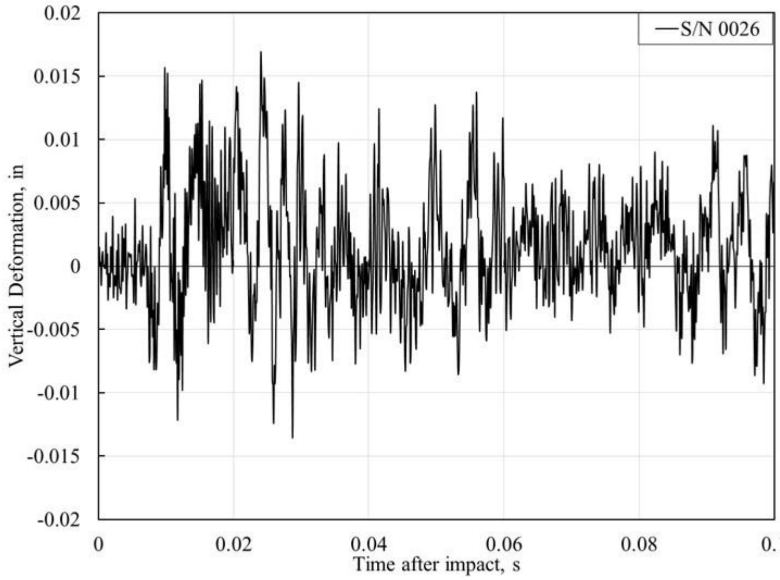

Figure 21. Time-history of average in-plane (vertical) deformation for Sideways modules (South view)

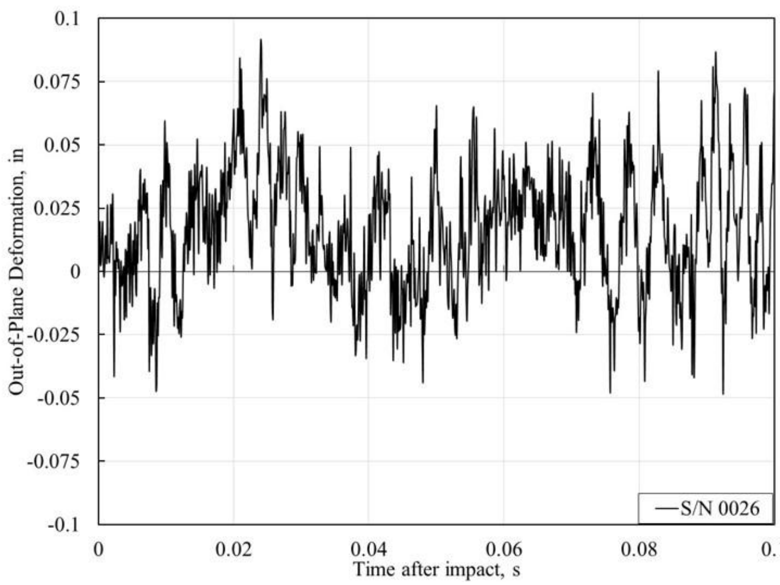

Figure 22. Time-history of average out-of-plane deformation for Sideways modules (South view)

The average in-plane (vertical) deformation was approximately ± 0.015 in, which is within the measurement uncertainty of the 3D-DIC system. The average out-of-plane deformation was approximately ± 0.08 in and exhibits a sinusoidal response, which was more than likely related to the aluminum baseplate bending. Note, the noise in the data was also likely related to insufficient lighting (darkness was approaching during the test), vibrations in the aluminum baseplate and/or surface artifacts of the module (i.e. fasteners and standoffs).

The in-plane (vertical) and out-of-plane deformation contour plots for the Rightside Up modules (East camera system) are shown next in Figure 23, along with the time-history of average displacement, Figure 24 and Figure 25. Again, the purple color represents the minimum value, while the red color represents the maximum value.

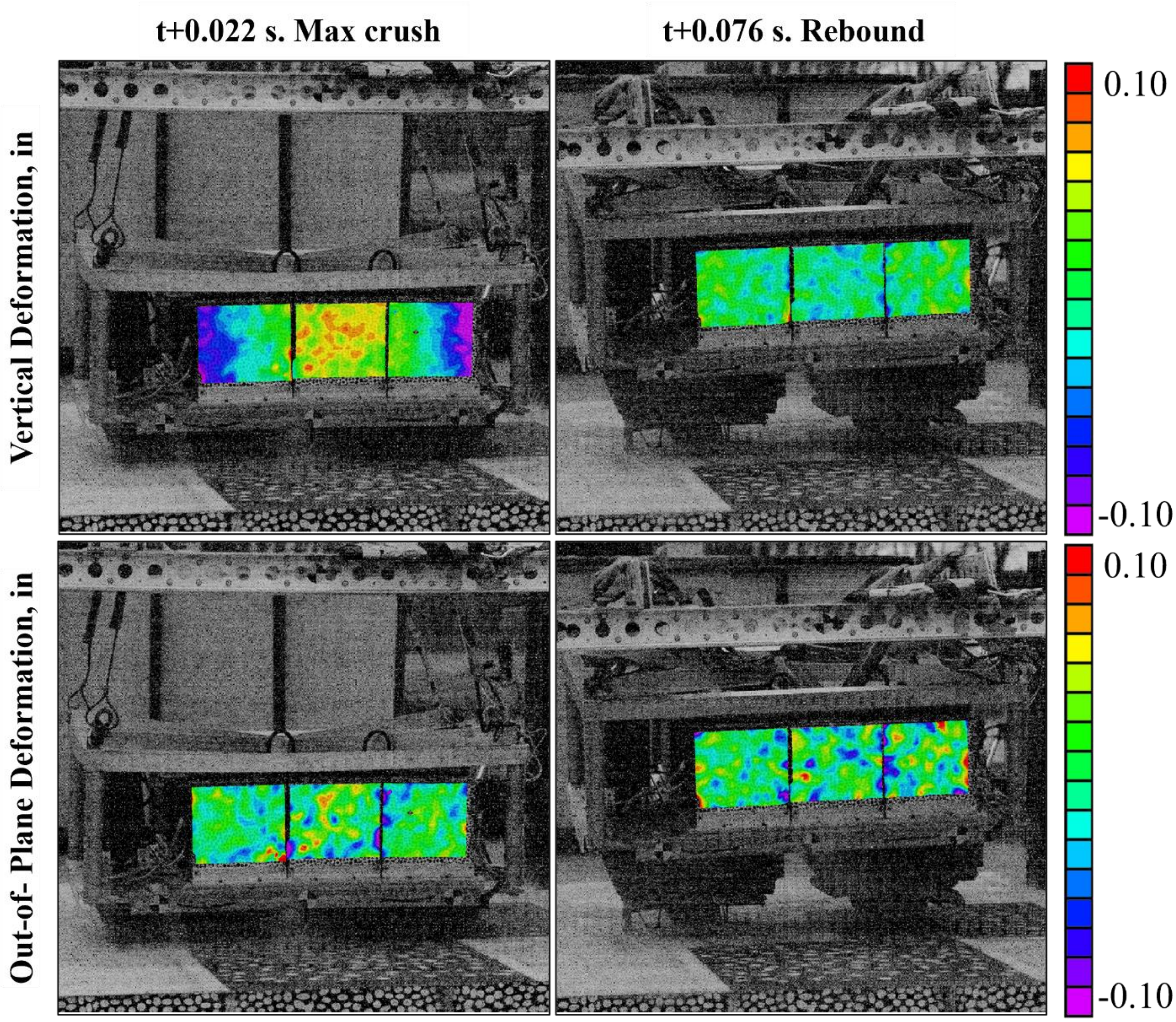

Figure 23. In-plane (vertical) and out-of-plane deformation contour plots for Rightside Up modules (East-view)

The Rightside Up modules exhibited a very rigid response and mimicked the deformation and bending of the aluminum baseplate, which is evident in the vertical deformation at maximum crush, t + 0.022 s. Curvature in the plate can be visually observed at this time, and the left (S/N 0008) and right (S/N 0021) modules exhibited downward deformation, as highlighted by the purple color. The module in the center, S/N 0036, exhibited an upward deformation, as highlighted by the red color. The overall magnitude of both the vertical deformation and out-of-plane deformation was approximately ± 0.10 in. An examination of the time-history of the average displacement, as measured across the entire surface of the module, provides a more complete understanding of the overall response. The time-history plots are shown next in Figure 24 and Figure 25.

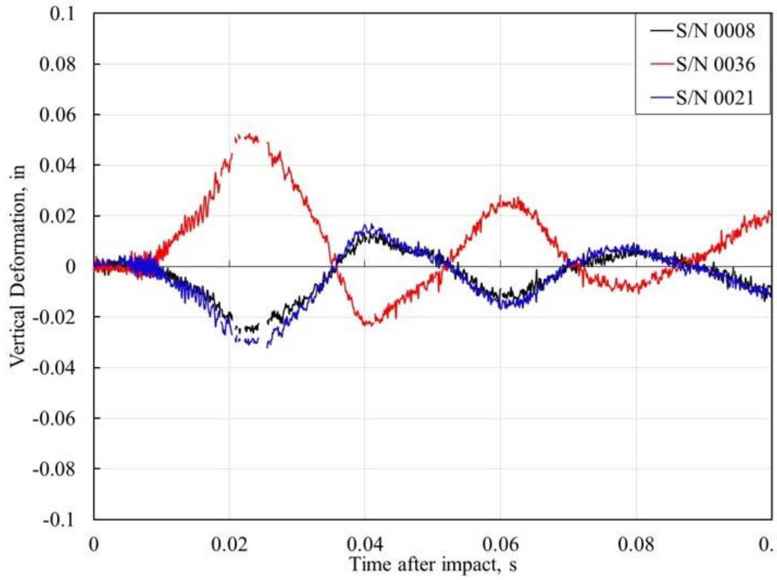

Figure 24. Time-history of average in-plane (vertical) deformation for Rightside Up modules (East view)

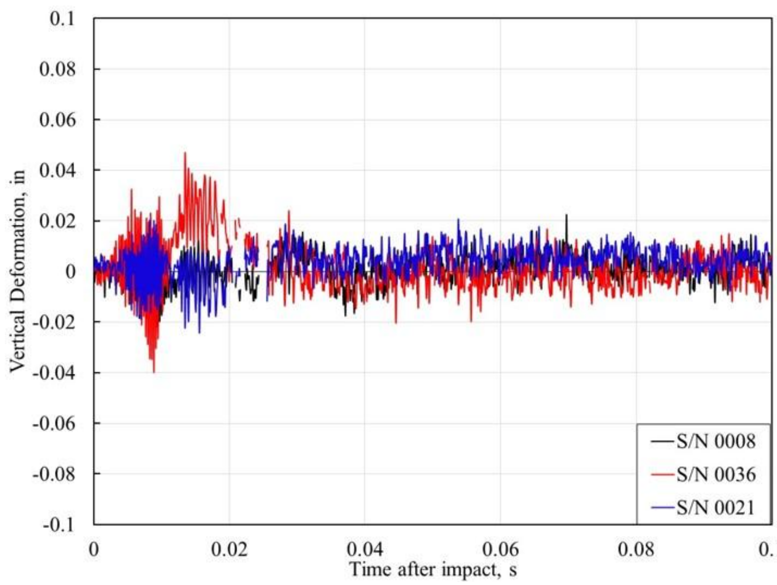

Figure 25. Time-history of average out-of-plane deformation for Rightside Up modules (East-view)

The average in-plane (vertical) deformation was approximately ± 0.050 in and exhibited a sinusoidal response, which was attributed to the aluminum baseplate bending. The average out-of-plane deformation was approximately ± 0.04 in, which occurred during the initial crushing of the paper honeycomb, prior to t = 0.022 s. After this time, the average out-of-plane deformation was approximately ± 0.015 in, which is within the measurement uncertainty of the photogrammetry system. Note, as before, the noise in the data was likely related to insufficient lighting (darkness was approaching during the test), vibrations in the aluminum baseplate and/or surface artifacts of the module (i.e. fasteners and standoffs).

Next the TC data were examined. The TC data starting approximately 3 minutes prior to impact and continuing throughout the impact event are shown in Figure 26.

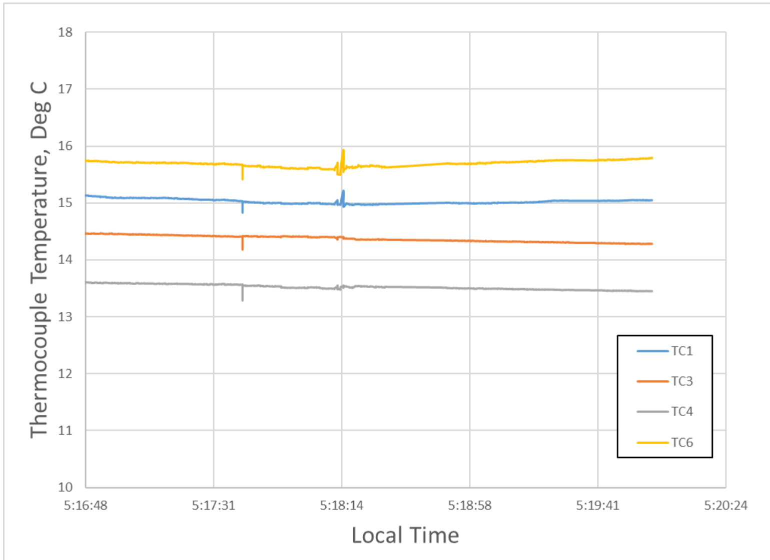

Figure 26. Thermocouple data at impact

Noting the impact time of 5:19, the four TCs that functioned nominally show a slight offset near the time of impact. (The two TCs with signal loss identified during pretest checkouts did not measure any temperature readings during the test, and thus their data plots are not shown). However, this signal appeared to be a momentary offset and settled back in line with the pre-test data. These results were confirmed by the BMU data, which did not register any effect from the impact in the logged temperature data. The BMU data is next shown in Figure 27.

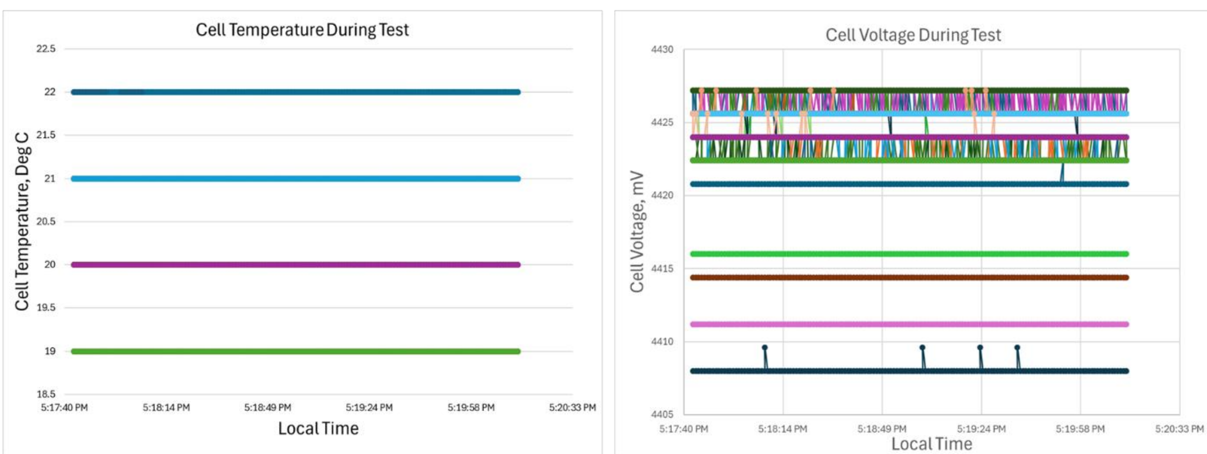

Figure 27. BMU data at impact. Cell temperature (left), and voltage (right)

Note the BMU data shows results from all 60 individual cells (10 per module, with 6 modules tested). The cell temperature data are shown on the left. Note all 60 cells are represented in the plot, with each of the cells falling to be one of the four temperatures measured, which ranged between 19- and 22-°C. There were no spikes or any other data that could be considered abnormal in the individual cell temperature responses around the time of impact, according to what was recorded in the BMU. The BMU also recorded individual cell voltage, is shown on the right graph. Again, all 60 cells are plotted, with cell voltages ranging between 4405 and 4420 mV, with multiple cells represented by each trace. As with the temperature data, there were no severe spikes or otherwise abnormal events that occurred at the time of impact. However, there were some cells that alternated between two voltage measurements, which is most visible in the bottom blue trace in the plot. However, these four spikes in the data were only an artifact of the BMU recording resolution and not from the test itself. The BMU recorded voltage with a resolution of 0.4 mV, so data having two distinct voltage values that alternated back and forth indicated voltage in the cell was somewhere between the two alternating values. No large spikes or jumps spanning multiple volts were evident in any of the data logged from the BMU.

The images from the IR cameras were next examined. One camera imaged the entire hour after the test, while the other only had limited memory and turned off approximately 20 minutes after the event. The IR camera located Southeast of the test article, primarily imaging the Rightside Up modules is shown first in Figure 28.

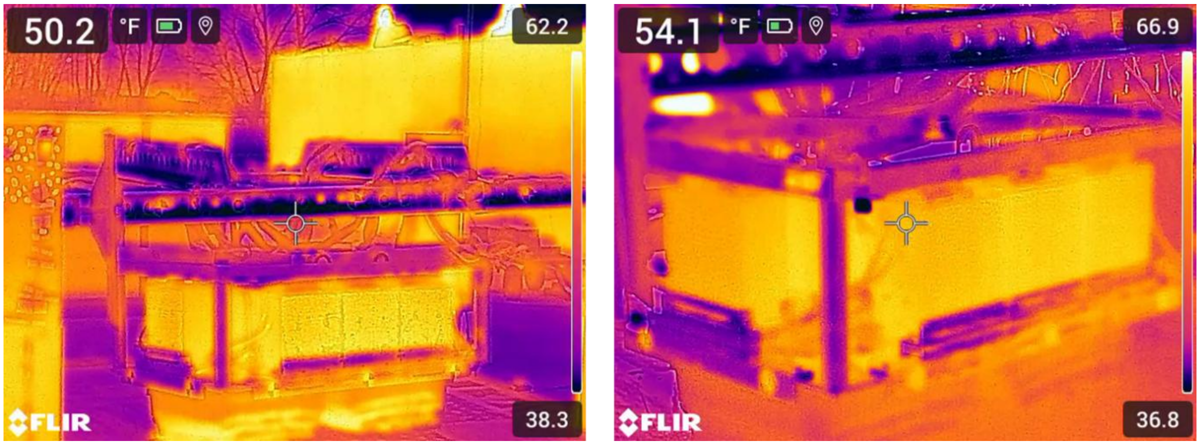

Figure 28. Southeast IR Camera data. Post-test (left) and t+1 hour post-test (right)

The camera was moved closer to the test article during the one-hour monitoring time to get a more detailed measurement. Temperature remained uniform in all the modules, with no notable events obtained. Next the thermal data from the Northwest IR camera was examined. It is shown in Figure 29.

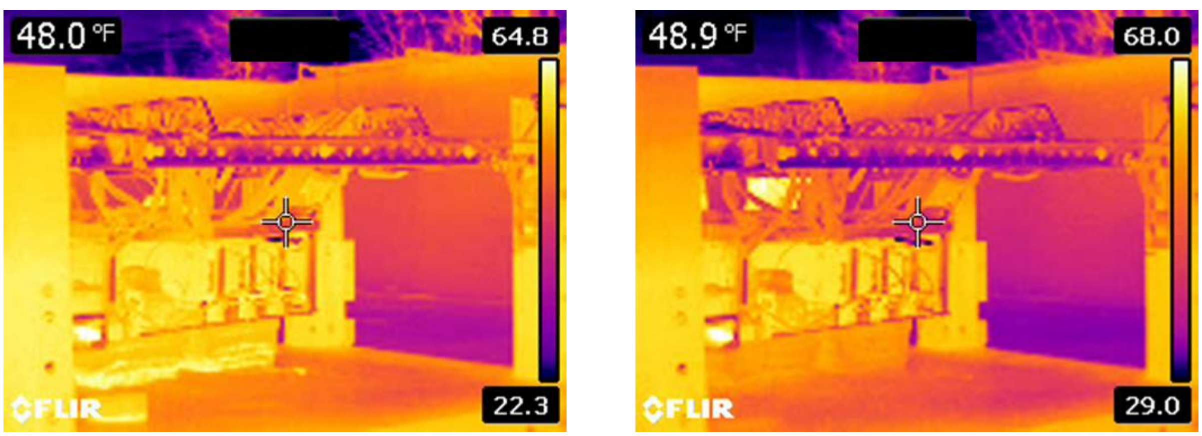

Figure 29. Northwest IR Camera data. Post-test (left) and approximately t+20 minutes (right)

As with the Southeast camera, the thermal images recorded from the Northwest camera showed approximately uniform surface temperatures on all the hardware recorded. This camera was also able to image portions of the BMU and MPD, however these are only partially visible, as they were partially obscured by the test rig post. This camera was stopped at t+20 minutes due to limited memory, but the data that was collected did not show any anomalies present. The TC data collected during the post-test monitoring period was next examined and is shown in Figure 30.

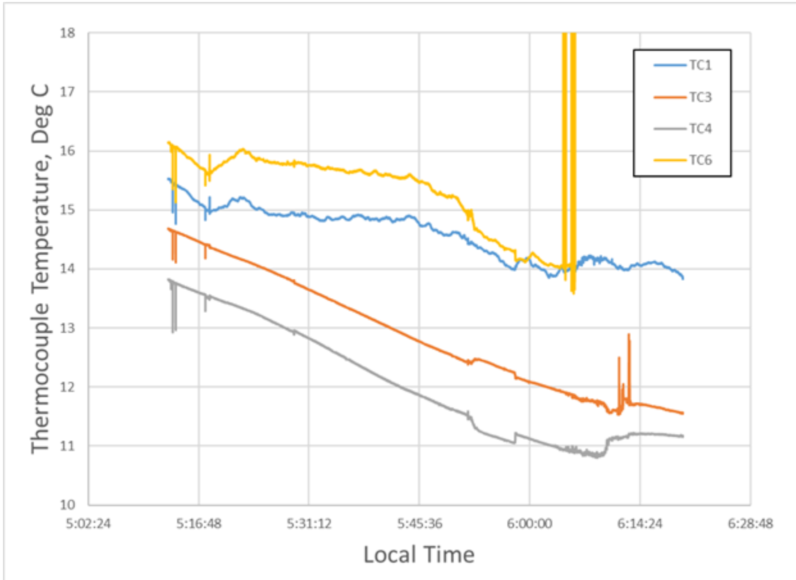

Figure 30. Thermocouple data for post-test monitoring

The post-test t+1 hour data shows gradually decreasing temperature from the four functioning thermocouples that were recording data. During this time, at approximately 6:05 PM local time, thermocouple #6 experienced some type of disturbance that caused its reading to saturate at its limits, which are not shown in Figure 30. During the post-test monitoring, test personnel were disassembling portions of the test site not critical to the post-test monitoring, and it was possible that a cable connection became lose or some other event occurred related to the test disassembly, which caused this disturbance. Since the other thermocouples were still recording nominal data, and both the thermal cameras and visual inspections that occurred at this time did not show any type of anomalous event, this data was discounted as a sensor error and not investigated further. This data was further confirmed by the post-test BMU data from all 60 of the cells, which is shown next in Figure 31.

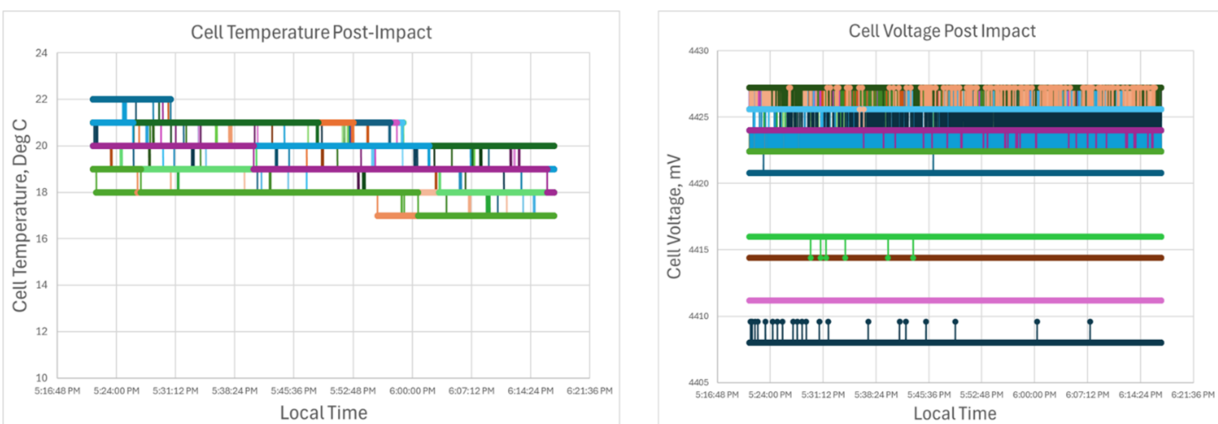

Figure 31. Post-test BMU data. Cell temperature (left) and voltage (right)

The data obtained from the BMU shows similar trends to that obtained from the thermocouples. Starting with the temperature data presented in Figure 31 (left), this data exhibited a downward trend of temperatures throughout the post-test monitoring period. The vertical lines in the data are an artifact of the resolution of the measurement (1 degree) collected and did not affect the overall trends. The overall trend showed the temperature in the cells gradually decreased as the post-test monitoring period progressed, which followed overall trends in the other data collected. When examining the cell voltage post-test, (Figure 31, right), the cell-level voltage for the 60 cells that were monitored remained steady during the pre-test timeframe and the post-test monitoring period. The cell level voltages ranged between 4408 mV and 4427.2 mV, which suggests the modules are in a nominal state. As with the temperature results, vertical lines in the data were artifacts of the resolution of the measurement (0.4 mV) and not indicative of cell instability.

After the post-test monitoring, the test article was removed from the test site and stored in outside storage for a period of 24 hours.

Post-Test Inspections

The test article was removed from outside storage on January 14, 2026. Querying the status by using the BMU showed the SoC of the system was still at 96%. The modules were then discharged prior to post-test inspections.

The initial step of the post-test teardown involved the disassembly and removal of the enclosure assembly, starting with the two rigid end caps from each module. A detailed visual and mechanical inspection was conducted to assess the structural response of the enclosures for the presence of dents, deformation or other signs of damage. The six enclosures are shown in Figure 32. Both the outer casing and the end caps exhibited structural integrity, showing no visible signs of plastic deformation. There was no evidence of buckling or fracturing at the fastener mounting points or shear distortion along the seam interfaces. It appeared the outer casing maintained its structural stability.

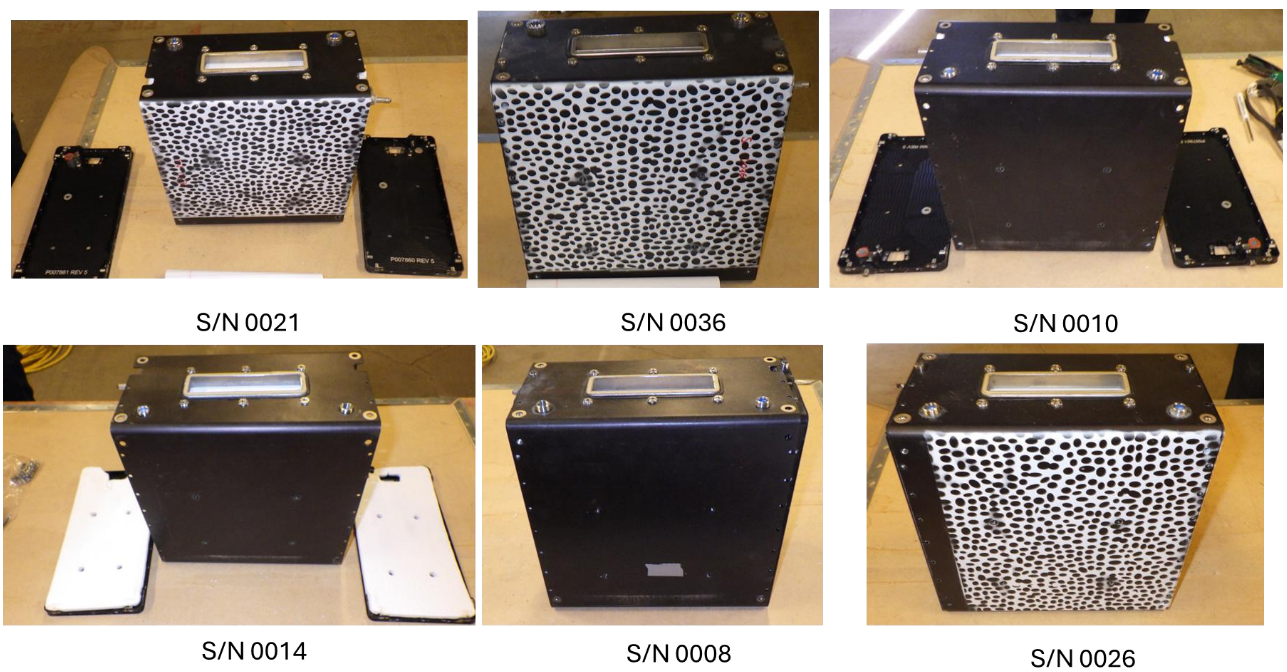

Figure 32. Post-test forensics. Enclosure assembly

Once the enclosure assembly was removed, the containment assembly was revealed, which showed the encapsulation designed to house the cells and serve as a thermal runaway propagation barrier. To access the containment assembly, the metallic foil layer was cut, thereby exposing the underlying thermal insulation material. Inspection of the mounting interfaces revealed no signs of material yield or fastener pull-out failure. The fasteners were all intact, with no protrusion, thread stripping, or localized indentation observed, which are shown in Figure 33. Furthermore, the thermal insulation layer remained intact, displaying no distinguishable abrasions or tears that would indicate damage from the impact.

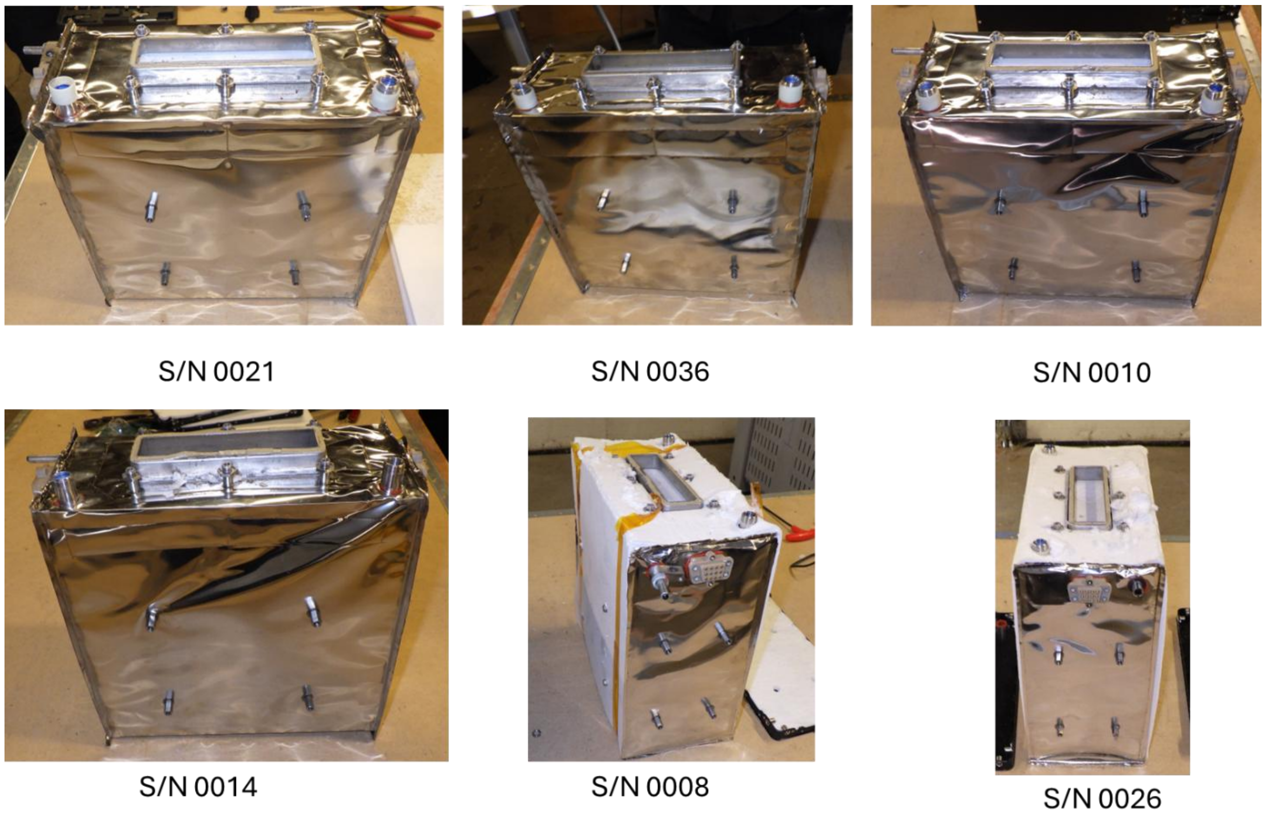

Figure 33. Post-test forensics. Containment assembly

After the removal of the containment assembly, the cell assembly was examined. The cell assembly included the internal bus bar network, the terminal lead ends of the module, the active coolant channel, and the internal plastic enclosure. The internal bus bar assembly, including electrical voltage and temperature leads, showed no external damage or connection severing. The primary module terminal leads also did not show signs of any visible damage. The internal plastic shell case known as the cell assembly appeared largely undeformed. Additionally, the metal inserts molded into the sides of the plastic enclosures remained seated, showing no signs of pull-out or protrusion. The module cell assemblies are shown in Figure 34.

Figure 34. Post-test forensics. Cell assembly

The final stage of the post-test inspection focused on the structural condition of the individual pouch cells. Accessing these cells required the removal of the internal plastic casing, which was structurally bonded to the cell assembly using an industrial silicone sealant. Due to its strength, residual sealant remained on the cell surfaces post-disassembly. Overall, the cells experienced negligible global deformation. The bottom profile of the pouch cells across all modules, which are shown in Figure 35, confirm the primary cell structures remained intact without evidence of swelling, folding, or internal shifting. While a few cells in each module exhibited very localized, minor deformation, this was likely a result from the mechanical prying forces required to separate the bonded plastic casing from the cell assembly. Ultimately, there was no consistent, module-wide deformation pattern that could be attributed to impact event itself.

Figure 35. Post test forensics. Cells (bottom view) S/N not recorded.

Discussion

The results presented are the culmination of the three-phase research program that was intended to study behavior of ESS systems undergoing dynamic impact testing. This plan was conducted utilizing actual ESS hardware configured in increasing levels of complexity and realism as the research plan progressed. The previous two phases of testing – on ESS modules without surrounding structure in various orientations, and within simulated structure at two orientations and impact levels – provided the basis and background in order to be able to conduct this fully instrumented energized pack-level impact test.

In Phase 1, testing was conducted on the modules themselves to investigate failure mechanisms that occur during drop testing under what are likely the most extreme circumstances. This data is valuable because it shows how the failure mechanisms can affect hazard development and can also provide correlation to laboratory type sub-scale testing, which is much easier to conduct. Having the Phase 1 data which can be used to correlate between the two will allow for additional understanding to be gained from conducting tests at the sub-scale level and how the subscale results affect the full-scale hazard development. Additionally, the information obtained regarding damage development and progression can be useful as input to computational model simulations. Thus, the test data can be used to ground simulations, which can then be used to simulate a variety of other test orientations and configurations. This can provide more insight into and a better understanding of how and when damage occurs and under what circumstances hazards develop.

In Phase 2, the results from Phase 1 were utilized as the basis for the test development matrix. This phase increased the complexity of the test setup by introducing the surrounding structure concept, which was influenced by a series of full-scale tests on an eVTOL vehicle concept, conducted at NASA LaRC. By combining the full-scale vehicle tests with the sub-scale data, the higher levels of the building block approach were investigated. The results from Phase 2 were collected and examined and were used as the basis for acceleration levels for Phase 3. These results from the Phase 2 testing led to the development of this Phase 3 test, which examined energized modules in a configuration more relevant to eVTOL aircraft such that data can be collected and commentary on hazards or other events that may occur in actual operation can be given.

All three phases of testing acquired data on the module deformation, loading environment, and internal component health, both through sensor data collection and post-test teardowns and forensic investigations. The data represents progression from a component level to a system level, which means these three test series fall somewhere in the middle of the common building block approach or test pyramid methodology. Beyond the research that has been conducted a part of these three phases, there is a significant amount of research conducted on ESS modules and more specifically the ESS cells themselves at the material level, some references of these can be found in [10]. The component level tests conducted in this research can be used to correlate to material level data at the base of the pyramid. At the other end of the spectrum, as stated above, NASA has conducted at least one test of ESS surrogate modules at the full-scale level, with one example being the Lift+ Cruise full-scale test (L+C #2) [17], so data acquired from this test series can be used in conjunction with full-scale data to generate a greater understanding of ESS performance during crash events.

Additionally, since this large data set now exists, considerations should be given to attempting to generate computational simulations of these types of systems in both non-destructive and destructive regimes. If additional testing was considered for this test series, it is suggested that a computational model be employed to help identify critical test parameters such as state of charge levels, orientations, and input loading levels. If these computational models can prove to be even partially predictive utilizing the data collected, there is space for additional considerations to be made for simulation in lieu of physical testing as a part of an OEM's certification effort.

The text in the current regulations regarding *surrounding structure* has been interpreted in this report to represent a specific configuration. This test was not a certification test, thus the results shown are based on the interpretations that the authors provide. Additionally, the authors note that caution should be exercised in extrapolating these results to all types, makes, models, and conditions of ESS. There are many factors that go into conducting this test in addition to those mentioned in this report, and the applicability of these factors should be defined and determined prior to conducting similar types of tests. Thus, the data presented in this report should be taken with certain caveats, and sound judgement should be used when interpolating or extrapolating the results presented.

Finally, the methodology of requiring a drop height which corresponds to an impact velocity without a specified loading level should be discussed. While there is heritage in the original fuel system requirement, the question regarding its applicability for ESS systems has still not been fully addressed. The research conducted is intended to be a part of the discussion because it has its basis in existing regulation. To the authors' knowledge, no other alternative has been presented. However, other examples exist. In seat certification requirements [19], velocity and acceleration levels are specified in order to recreate a loading condition. These values have been established from historical data and testing. It is understood that the new 14 CFR § 23 Amendment 64 offers other avenues to address the requirement [20], however the prescribed testing is still one of them. Using this methodology, the ESS systems could utilize a parameter that involves both a drop velocity but also a loading level more applicable for aircraft environment. The results shown and discussion provided hopefully will provide some guidance should this idea be considered. As the previous paragraph states, surrounding structure was utilized for the test. It could be interpreted that utilizing surrounding structure in the test may be one mechanism used to define the loading level used in the test.

The data collected from this effort demonstrates that an ESS system can survive a 50-ft impact test when accounting for representative vehicle structure in the impact. The question still remains whether the 50-ft drop height is the best method for certification, and this study presents at least one data set for consideration. There are still factors that are outstanding related to the configuration of the test itself. Items such as the surrounding structure and assumption of loading levels, the level of state of charge on the modules, the additional equipment necessary and whether they should be under load are all considerations that are presented and factors for future discussion. The tests do, however, show a method for conducting a requisite 50-ft drop test by developing procedures, acquiring data, and evaluating the types of responses.

Summary

A dynamic drop test was conducted on six energized ESS modules and supporting hardware at the NIAR outdoor test stand in January 2026. The modules were placed on a base plate and subjected to a 100-g input deceleration value based on a literature review of relevant crash data. The test was conducted by attaching the base plate to a guided drop trolley which was lifted and dropped from a height of 50 feet.

The modules survived the test without any apparent visible, structural or electrical damage. Various methods were introduced to monitor and record data from variety of sources including external temperature and acceleration sensors connected to DAS systems. Additionally, internal cell health in the form of voltage and temperature data was logged prior to, during, and after the test by the BMU itself. Finally, after determining it was safe to do so, inspections were conducted by disassembling each module down to the cell level. Post-test inspections of the BMU and MPD revealed no damage, hazards or other off nominal behavior that would cause faults in the units. The test data has been collected, examined, and is presented in this report.

The data collected is intended to improve the state-of-the-art in ESS testing along with providing some answers to help guide regulatory development. This test campaign provided the authors with a chance to gain knowledge and experience with ESS systems, test conduct, and applicable regulations which can be used for future project planning and testing. Much of this knowledge has also been disseminated in various publications via publicly available avenues. It is hoped the rationale used, lessons learned, techniques developed, the data collected, and the discussion presented can be used to better inform all interested parties such that the goals of a fully healthy AAM ecosystem can be realized.

Acknowledgements

The authors would like to thank Rob Huculak and his test team at NIAR for conducting the test. In addition, the authors would like to thank Joseph James, Benjamin Hansen and Thomas Hartmann at EPS for the test support, technical data and for assisting in conducting post-test forensics.

References

1. FAA. “The eIPP: What You Need to Know.” March 9, 2026. https://www.faa.gov/newsroom/eipp-what-you-need-know. Accessed March 11, 2026.

2. Federal Register. “Airworthiness Criteria: Special Class Airworthiness Criteria for the Joby Aero, Inc. Model JAS4–1 Powered-Lift.” Volume 89, No. 47. Pages 17230-17264. March 8, 2024.

3. Federal Register. “Airworthiness Criteria: Special Class Airworthiness Criteria for the Archer Aviation Inc. Model M001 Powered-Lift.” Volume 89. No. 102. Pages 45944-45977. May 24, 2024.

4. Code of Federal Regulations. “Designation of Applicable Regulations.” 14 CFR §21.17 Paragraph b. Last Amended Feb 16, 2024.

5. EASA. “Small Category VCA revision 0.” October 2024.

6. EASA. “Fuel System Crash Resistance.” CS 27.952. CS 27 Amendment 10. February 2023.

7. Code of Federal Regulations. “Fuel System Crash Resistance.” 14 CFR §27.952. October 3, 1994.

8. NIAR-WSU. “NIAR conducts 50-ft eVTOL battery drop test per 14 CFR § 27.952.” December 2, 2022. https://www.wichita.edu/industry_and_defense/NIAR/MediaCenter/2022-12-22.php. Accessed May 5, 2025.

9. Archer. “Archer Successfully Completes Multiple Battery Pack Drop Tests; One of the Most Challenging Tests It Is Set to Face as Part of the FAA’s Type Certification Program.” https://investors.archer.com/news/news-details/2024/Archer-Successfully-Completes-Multiple-Battery-Pack-Drop-Tests-One-of-the-Most-Challenging-Tests-It-Is-Set-to-Face-as-Part-of-the-FAAs-Type-Certification-Program/default.aspx. Accessed March 9, 2026

10. Littell, J.D., Gardner, N.W., and Ellafrits, S.A. “Dynamic Testing of eVTOL Energy Storage Systems: Literature Review and Path Forward.” NASA TM 20220015117. January 2023.

11. Littell, J.D. et al. “Dynamic Drop Testing of eVTOL Energy Storage Systems Part 1: Drop Test Data Summary.” Proceedings from Vertical Flight Society’s 81st Annual Forum & Technology Display, May 20-22, 2025, Virginia Beach, Virginia.

12. Littell, J.D. et al. “Dynamic Drop Testing of eVTOL Energy Storage Systems Part 2: Deformation and Post-Test Forensics Results.” Proceedings from Vertical Flight Society’s 81st Annual Forum & Technology Display, May 20-22, 2025, Virginia Beach, Virginia.

13. Littell, J.D. et al. “A Summary of Results from Phase 2 Dynamic Drop Testing of Energy Storage Systems for Vertical Take-off and Landing (eVTOL) Vehicles.” NASA TM 20250006515. July 2025.

14. Federal Aviation Administration. “Technical Standard Order: Rechargeable Lithium Batteries and Battery Systems.” TSR-C179b. March 23, 2018.

15. United Nations. “Manual of Tests and Criteria, Seventh Revised Edition.” ST/SG/AC.10/11/Rev 7. 2019.

16. Littell, J.D. and Putnam, J.B. “A Summary of Test Results from a NASA Lift + Cruise eVTOL Crash Test.” Proceedings from the Vertical Flight Society’s 79th Annual Forum & Technology Display, May 16-18, 2023, West Palm Beach, Florida.

17. Littell, J.D., et al. “A Summary of Test and Analysis Results from a Second Lift+Cruise Full-Scale Drop Test.” NASA TM. NASA/TM-20260003620. May 2026.

18. Society of Automotive Engineers (SAE). “Surface Vehicle Recommended Practice: Instrumentation for Impact Test-Part 1-Electronic Instrumentation.” SAE J211-1. 2007.

19. Federal Aviation Administration. “Emergency Landing Dynamic Conditions.” 14 CFR § 27.562. Amended November 13, 1989.

20. AOPA. Understanding Part 23 Rewrite. https://www.aopa.org/advocacy/advocacy-briefs/understanding-part-23-rewrite. Accessed April 6, 2026.